LUND UNIVERSITY

Quantification of Fat Content and Fatty Acid Composition Using Magnetic Resonance Imaging

Peterson, Pernilla

2013

Quantification of Fat Content and Fatty Acid Composition Using Magnetic Resonance Imaging

Pernilla Peterson

LUNDS UNIVERSITET

DOCTORAL DISSERTATION

by due permission of the Faculty of Medicine, Lund University, Sweden.

To be defended in Lilla aulan, Jan Waldenströms gata 5, Malmö, Friday Dec 13th 2013 at 13.00.

Faculty opponent

Asst. Prof. Houchun Harry Hu, Radiology & Imaging Services, Children's Hospital Los Angeles

Organization	Document name
LUND UNIVERSITY	DOCTORAL DISSERTATION
Medical Radiation Physics	Date of issue
Department of Clinical Sciences, Malmö	Nov 22nd 2013
Author(s)	Sponsoring organization
Pernilla Peterson	

Title and subtitle
Quantification of Fat Content and Fatty Acid Composition Using Magnetic Resonance Imaging

Abstract

In obesity and several other disease scenarios, the measurement of fat accumulation in various organs and tissues has become a sought-after technique in clinical diagnostics and research. Especially, quantitative and non-invasive techniques which also provide images of accumulated fat throughout the body would be valuable. In the typical hospital, magnetic resonance imaging (MRI) is the only technique available which has the potential for these types of measurements and out of techniques suggested, Water/Fat Imaging is particularly promising. Water/Fat Imaging is based on the separation of water and fat, the two main contributors to the MRI signal, with the use of the frequency separation between their signals. The field has inspired a wide range of research and is by now well established, especially for investigations of fatty liver. However, in this and several other applications there is a continued need for method development.

The fat concentrations in skeletal muscle are expected to be very low. Thus, for this application, there is an increased demand for measurement precision. The results presented in this thesis indicate that fat concentrations below 1 % are possible to measure using Water/Fat Imaging. In addition, precision may be increased using a higher flip angle if a pure fat reference is used for quantification, without compromising quantification accuracy. (**Papers I and II**)

Water/Fat Imaging has become an appreciated technique for abdominal applications in which breath-hold is necessary for acceptable image quality. The use of a bipolar acquisition scheme may be used to reduce the total scan time, but is associated with issues which are detrimental to fat quantification. Using a built-in correction approach, it is demonstrated that accurate and noise efficient fat quantification is possible using a bipolar acquisition. (**Paper III**)

The basic ideas of Water/Fat Imaging may be extended to not only quantify the fat concentration, but also the fatty acid composition. In this thesis, a reconstruction algorithm is suggested and its accuracy is demonstrated in a wide range of fat concentrations and fatty acid compositions. In addition, a number of potential sources of bias are investigated. Out of these, accurate modeling of the individual T_2 values of fat and water is especially important in fat/water mixtures, whereas some T_1 weighting may be allowed with small impact on quantification accuracy. (**Papers IV and V**)

Key words: MRI, fat quantification, water/fat imaging, chemical shift, skeletal muscle, fat reference, bipolar gradient, fatty acid composition, relaxation

Classification system and/or index terms (if any)

Supplementary bibliographical information	Language: English

ISSN and key title: 1652-8220	ISBN: 978-91-87651-99-1

Recipient's notes	Number of pages: 82	Price
	Security classification	

Signature _____ Date Nov 4th 2013

Quantification of Fat Content and Fatty Acid Composition using Magnetic Resonance Imaging

Pernilla Peterson

LUNDS UNIVERSITET

Cover photo: Anders Turstam

Till min familj:

"Jag kunde ju!"
/ Pernilla Peterson, ca. 1986

Abstract

In obesity and several other disease scenarios, the measurement of fat accumulation in various organs and tissues has become a sought-after technique in clinical diagnostics and research. Especially, quantitative and non-invasive techniques which also provide images of accumulated fat throughout the body would be valuable. In the typical hospital, magnetic resonance imaging (MRI) is the only technique available which has the potential for these types of measurements and out of techniques suggested, Water/Fat Imaging is particularly promising. Water/Fat Imaging is based on the separation of water and fat, the two main contributors to the MRI signal, with the use of the frequency separation between their signals. The field has inspired a wide range of research and is by now well established, especially for investigations of fatty liver. However, in this and several other applications there is a continued need for method development.

The fat concentrations in skeletal muscle are expected to be very low. Thus, for this application, there is an increased demand for measurement precision. The results presented in this thesis indicate that fat concentrations below 1 % are possible to measure using Water/Fat Imaging. In addition, precision may be increased using a higher flip angle if a pure fat reference is used for quantification, without compromising quantification accuracy. (**Papers I and II**)

Water/Fat Imaging has become an appreciated technique for abdominal applications in which breath-hold is necessary for acceptable image quality. The use of a bipolar acquisition scheme may be used to reduce the total scan time, but is associated with issues which are detrimental to fat quantification. Using a built-in correction approach, it is demonstrated that accurate and noise efficient fat quantification is possible using a bipolar acquisition. (**Paper III**)

The basic ideas of Water/Fat Imaging may be extended to not only quantify the fat concentration, but also the fatty acid composition. In this thesis, a reconstruction algorithm is suggested and its accuracy is demonstrated in a wide range of fat concentrations and fatty acid compositions. In addition, a number of potential sources of bias are investigated. Out of these, accurate modeling of the individual T_2 values of fat and water is especially important in fat/water mixtures, whereas some T_1 weighting may be allowed with small impact on quantification accuracy. (**Papers IV and V**)

Populärvetenskaplig sammanfattning

Fetma har blivit ett växande folkhälsoproblem under de senaste decennierna och den epidemiartade utvecklingen har fått stor uppmärksamhet. Faktum är att världshälsoorganisationen WHO uppger att 1.4 miljarder människor är överviktiga och att 65 % av jordens befolkning lever i länder där fler dör av övervikt och fetma än av undervikt. Fetma är nära kopplat till hjärt- och kärlsjukdom och diabetes, men hur stor risken är beror på var i kroppen fettet lagras och hur det är sammansatt. Till exempel anses fettansamling i eller mellan organ mer allvarligt än ett rejält lager underhudsfett, och fettets kemiska sammansättning skulle kunna skvallra om inflammatoriska tillstånd.

Inom forskning och diagnostik av fetma och andra fettrelaterade sjukdomar räcker alltså badrumsvågen inte till. Det räcker inte att veta hur feta vi är – vi måste veta var vi är feta och hur fettet är sammansatt. Det behövs därför detaljerade och noggranna mätningar av mängden fett och av dess kemiska sammansättning. För att kunna undersöka var fettet finns lagrat behövs en bildgivande metod. För att kunna upprepa mätningarna för att följa ett sjukdomsförlopp eller effekten av en behandling, är det dessutom en fördel om mätningarna kan göras utan ingrepp i kroppen och utan röntgenstrålning. Av de diagnostiska verktyg som finns tillgängliga på sjukhus, är fettmätningar med magnetkamera det enda som lever upp till alla dessa önskvärda egenskaper.

En av de viktigaste egenskaperna hos en magnetkamera är dess förmåga att avbilda mjukdelar. Magnetkameran tar bilder av väteatomerna i våra kroppar och framförallt är det vätet i våra vatten- och fettmolekyler som syns. Med metoden vatten/fett-avbildning kan magnetkamerans bilder sorteras så att bilden av vatten och bilden av fett kan ses var för sig. Från dessa separata vatten- och fettbilder kan vi därefter beräkna den procentuella koncentrationen av fett.

Det första fröet till vatten/fett-avbildning såddes 1984 och under åren som följt har metoden genomgått en stor utveckling. Metoden kan nu användas för att göra noggranna mätningar av fettkoncentrationen i exempelvis levern, ett organ som ofta drabbas när underhuden inte längre kan lagra mer fett. Det finns till och med de som spekulerar i om metoden är mer pålitlig än vävnadsprover tack vare möjligheten att titta på hela organet och att göra exakta mätningar. Det kan alltså vara dags att tänja på gränserna och undersöka vad metoden mer kan erbjuda. I det här avhandlingsarbetet har jag gjort just detta. Jag har utvecklat metoden vidare för att kunna mäta riktigt låga

fettkoncentrationer. Jag har också undersökt en mer effektiv bildtagningsmetod, samt tagit fram en metod som kan undersöka fettets kemiska sammansättning.

Även mycket låga fettkoncentrationer kan ha stor betydelse i muskler. För att kunna mäta dessa små mängder är det dock viktigt att magnetkamerans bilder inte är alltför brusiga och att vår beräkning är så noggrann och exakt som möjligt. Genom att ta hänsyn till detta har jag kunnat mäta fettkoncentrationer så låga som 0.5 % i provrör, och genomfört noggranna och exakta mätningar i muskler hos friska personer och patienter med lymfödem.

För att bilderna inte ska bli suddiga av patientens andningsrörelser är det vid bildtagning i buken viktigt att bildtagningen är tillräckligt snabb för att patienten ska kunna hålla andan. En effektivare bildinsamling finns tillgänglig med vanlig magnetkamerautrustning, men bilderna har hittills inte kunnat användas för beräkningar av fettinnehållet. Jag har visat att en korrigerad beräkning gör det möjligt att använda även dessa, mer effektivt insamlade, bilder för noggranna fettmätningar.

I detta avhandlingsarbete har jag också tagit fram en metod för att undersökta fettets kemiska sammansättning med samma typ av bilder och teknik som används för vatten/fett-avbildning. Jag har granskat vilka möjliga felkällor av mätningarna som är viktiga att ta hänsyn till och kunnat genomföra noggranna mätningar i provrör och i mänsklig fettvävnad.

Vatten/fett-avbildning är ett flexibelt och noggrant verktyg för att mäta koncentrationen fett och dess kemiska sammansättning i människokroppen. Framförallt är mätning av den kemiska sammansättningen ett spännande fält för fortsat utvecklingsarbete, medan mätningen av fettkoncentrationen är redo för att användas i diagnostik och forskning om fetma och andra fettrelaterade sjukdomstillstånd.

Abbreviations

BMI	Body mass index
bSSFP	Balanced steady-state free precession
cl	Chain length
CRB	Cramér-Rao Bound
CT	Computed tomography
DECT	Dual-energy computed tomography
DEXA	Dual-energy X-ray absorptiometry
EMCL	Extramyocellular lipids
FF	Fat fraction
fFF	Fat reference fat fraction
GRASE	Gradient- and spin echo
IMAT	Intermuscular adipose tissue
IMCL	Intramyocellular lipids
MANA	Multi scale adaptive averaging
MR	Magnetic resonance
MRI	Magnetic resonance imaging
MRS	Magnetic resonance spectroscopy
NAFLD	Non-alcoholic fatty liver disease
NASH	Non-alcoholic steatohepatitis
ndb	Number of double bonds
nmidb	Number of methylene-interrupted double bonds
NSA	Effective number of signal averages
PRESS	Point-resolved spectroscopy
RF	Radio frequency
SNR	Signal-to-noise ratio
STEAM	Stimulated echo acquisition mode
TR	Repetition time
VAT	Visceral adipose tissue

List of symbols

a	Flip angle [°]
$\mathbf{A}_{NxP}$	Signal evolution matrix
$\mathbf{B}$	Error estimation matrix
B_0	Main magnetic field [T]
B_1	Radio-frequency field [T]
$\mathbf{D}_{NxN}$	Off-resonance matrix
E_m	Exponential term expressing the phase evolution of the mth fat peak
G_x	Read-out gradient
I	Number of measurements
K	Normalization factor of the theoretical fat resonance amplitudes
M	Number of fat resonances
N	Number of echoes
P	Number of parameters to be estimated
$\mathbf{S}_{Nx1}$	Signal matrix
S_{IP}	In-phase signal
S_n	Signal of the nth echo
S_{OP}	Opposed-phase signal
SD_{ftv}	Standard deviation from the true value
T_1	Longitudinal relaxation time [s]
$T_{1f,w}$	T_1 of the fat or water signal, respectively [s]
T_2	Intrinsic transverse relaxation time [s]
$T_{2f,w}$	T_2 of the fat or water signal, respectively [s]
T_2^*	Effective transverse relaxation time [s]
T_2'	Extrinsic transverse relaxation time [s]
t_n	Echo time of the nth echo [s]
V	Number of voxels
α_m	Relative amplitude of the mth fat resonance [au]
Δf_m	Chemical shift of the mth fat resonance relative to water [Hz]
Δt	Inter-echo time [s]
$\Delta\tilde{\theta}$	Error of the estimated complex field map [rad]
$\Delta\tilde{\rho}_{f,w}$	Error of the estimated parameter $\tilde{\rho}_{f,w}$ [au]
$\Delta\tilde{\psi}$	Error of the estimated parameter $\tilde{\psi}$ [Hz]

ε	Amplitude modulation [au]
θ	Complex error
$\mathbf{\Theta}_{NxN}$	Complex error matrix
$\mathbf{\rho}_{Px1}$	Vector matrix of parameters to be estimated
$\tilde{\mathbf{\rho}}_{Px1}$	Estimate of the matrix $\mathbf{\rho}_{Px1}$
ρ	Estimated parameter
$\rho_{f,w}$	Fat or water signal, respectively [au]
$\tilde{\rho}_{f,w}$	Estimate of the fat or water signal, respectively [au]
$\rho_{f0,w0}$	Unweighted fat or water signal, respectively [au]
σ_ρ^2	Variance of the estimated parameter
σ_S^2	Variance of the raw data signal
ϕ	Phase error [rad]
ψ	Off-resonance frequency [Hz]
$\tilde{\psi}$	Estimate of the off-resonance frequency [Hz]
$\hat{\psi}$	Complex field map [Hz]

Original papers

The thesis is built on the following papers, which will be referred to by their Roman numerals:

I. **Quantification of Low Fat Contents: a Comparison of MR Imaging and Spectroscopy Methods at 1.5 and 3 T**. Sven Månsson, <u>Pernilla Peterson</u>, and Edvin Johansson. *Magnetic Resonance Imaging*, 30(10):1461-1467 (2012)

II. **Fat Quantification in Skeletal Muscle Using Multigradient-Echo Imaging: Comparison of Fat and Water References**. <u>Pernilla Peterson</u>, Thobias Romu, Håkan Brorson, Olof Dahlqvist Leinhard, and Sven Månsson. *Manuscript*.

III. **Fat Quantification Using Multi-Echo Sequences with Bipolar Acquisition: Investigation of Accuracy and Noise Performance**. <u>Pernilla Peterson</u> and Sven Månsson. *Magnetic Resonance in Medicine,* In press, doi: 10.1002/mrm.24657 (2013)

IV. **Simultaneous Quantification of Fat Content and Fatty Acid Composition using MR imaging**. <u>Pernilla Peterson</u> and Sven Månsson. *Magnetic Resonance in Medicine*, 69(3):688-697 (2013)

V. **Relaxation Effects in MR Imaging-Based Quantification of Fat Content and Fatty Acid Composition**. <u>Pernilla Peterson</u>, Jonas Svensson, and Sven Månsson. *Accepted for publication in Magnetic Resonance in Medicine* (2013)

Published papers have been reproduced with kind permission from Elsevier Limited (**Paper I**) and John Wiley and Sons (**Papers III and IV**).

Preliminary reports

The following preliminary reports were given at international meetings:

i. **Quantification of Low Fat Contents: a Comparison Between MR Imaging and Spectroscopy Methods at 1.5 and 3 T**. <u>Pernilla Peterson</u>, Edvin Johansson, and Sven Månsson. *26th Annual Meeting of the European Society for Magnetic Resonance in Medicine and Biology (ESMRMB)*, Antalya, Turkey, 2009

ii. **Quantification of Fatty Acid Compositions Using MR-Imaging and Spectroscopy at 3 T**. <u>Pernilla Peterson</u>, Håkan Brorson, and Sven Månsson. *Joint Annual Meeting of the International Society for Magnetic Resonance in Medicine (ISMRM) and the European Society for Magnetic Resonance in Medicine and Biology (ESMRMB)*, Stockholm, Sweden, 2010

iii. **Simultaneous Quantification of Fat Fraction and Fatty Acid Composition Using MRI**. <u>Pernilla Peterson</u> and Sven Månsson. *19th Annual Meeting of the International Society for Magnetic Resonance in Medicine (ISMRM)*, Montréal, Canada, 2011

iv. **Investigation of Subfascial Fat in Arm Lymphedema Using MRI-Based Fat Quantification**. <u>Pernilla Peterson</u>, Håkan Brorson, and Sven Månsson. *23rd International Congress of the International Society of Lymphology (ISL)*, Malmö, Sweden, 2011

v. **Fat Quantification with Built-In Phase Correction for Multi-Echo Acquisition with Bipolar Gradients**. Angelo Olsson, <u>Pernilla Peterson</u>, and Sven Månsson. *28th Annual Meeting of the European Society for Magnetic Resonance in Medicine and Biology (ESMRMB)*, Leipzig, Germany, 2011

vi. **Effect of Fat Content on Transversal and Longitudinal Relaxation Times of Fat and Water in Emulsion**. <u>Pernilla Peterson</u> and Sven Månsson. *28th Annual Meeting of the European Society for Magnetic Resonance in Medicine and Biology (ESMRMB)*, Leipzig, Germany, 2011

vii. **MR for Quantitative Fat Imaging**. <u>Pernilla Peterson</u> and Sven Månsson. *Medical Physics in the Baltic States 9*, Kaunas, Lithuania, 2011

viii. **Comparison of Accuracy and Precision of Image-Based Fat Quantification with Different Flip Angle Approaches in Skeletal Muscle**. Pernilla Peterson and Sven Månsson. *21st Annual Meeting of the International Society for Magnetic Resonance in Medicine (ISMRM)*, Salt Lake City, USA, 2013

ix. **Magnetic Resonance Imaging Shows Increased Content of Fat and Muscle/Water in Arm and Leg Lymphedema**. Pernilla Peterson, Håkan Brorson, and Sven Månsson. *24th International Congress of the International Society of Lymphology (ISL)*, Rome, Italy, 2013

Table of contents

1. Introduction

The prevalence of obesity has reached epidemic-like proportions with 1.4 billion of the world population being overweight in 2008 and 65 % living in countries where obesity causes higher mortality than underweight (World Health Organization 2013). In its path follows increased prevalence of several other disease conditions such as type 2 diabetes mellitus (Snel *et al.* 2012) and cardiovascular disease (Perez Perez *et al.* 2007). Apart from an excess of adipose tissue, obesity and its co-mortalities may also lead to fat accumulation in other organs, such as the liver, pancreas, and muscle (Rasouli *et al.* 2007). Accumulation of fat in adipose tissue and other organs is of interest also in several other diseases, such as inflammatory conditions (Pond 2005), lymphedema (Pond 2005, Brorson *et al.* 2006, Brorson *et al.* 2009), and conditions of chronic pain (Elliott *et al.* 2011). Thus, the growing recent interest in methods for measurements of the human fat is well motivated by an increasing need in diagnostics and research.

Fat measurements is a broad term which may aim at answering several different questions requiring various level of detail. For identification of groups of various risk profiles in obesity, it is relevant to identify and quantify the volume of various fat depots throughout the body (Rasouli *et al.* 2007). Quantification of fat concentration within a specific organ is of great importance in the diagnosis of e.g. non-alcoholic fatty liver disease (NAFLD); a condition which may lead to inflammation, cirrhosis, or even cancer (Snel *et al.* 2012). In even more detail, the chemical composition of the accumulated fat is dependent not only on the diet (Hodson *et al.* 2008), but also on adipose tissue depot (Malcom *et al.* 1989, Lundbom *et al.* 2011), inflammatory conditions (Pond 2005), and insulin sensitivity (Iggman *et al.* 2010).

For fat measurements to be truly valuable, the technique used should live up to several desirable properties. To enable comparison of repeated measurements, the measurement should be quantitative and non-invasive, and as both the fat concentration and the composition of fat may be heterogeneously distributed within an organ (Capitan *et al.* 2012, Lundbom *et al.* 2013), spatial information is valuable. Thus, an imaging-based method which non-invasively provides the fatty acid composition or percentage of fat on a continuous scale in each image voxel would be very useful.

Because of the invasive nature and the limited resolution of biopsies, and the difficulties in obtaining voxel-by-voxel quantitative fat measurements using ultrasound and computed tomography, magnetic resonance imaging (MRI) is the only diagnostic tool

available in the hospital that has the potential for both non-invasive and quantitative fat measurements. By cleverly controlling the acquisition and processing of MR images, it is possible to go beyond imaging of anatomy and obtain quantitative measures of the physical properties of the human body. The quantification of fat is one example, and its success depends on both the acquisition scheme and the method for post-processing of the images. Especially, much effort has been put into the development of the chemical-shift-encoded techniques which throughout this thesis will be referred to as Water/Fat Imaging (Dixon 1984, Reeder *et al.* 2004, Hu *et al.* 2012). Water/Fat Imaging methods have been used for a number of applications such as quantification of fat in the liver (Reeder *et al.* 2011), cardiac muscle (Kellman *et al.* 2010, Liu *et al.* 2010), skeletal muscles (Karampinos, Baum*, et al.* 2012), and pancreas (Hu *et al.* 2010). In addition, the techniques have proven to correlate very well to independent quantitative techniques (Hines *et al.* 2010, Hines *et al.* 2012). Thus, it may be time to explore the limit of what Water/Fat Imaging methods can do.

Measurements of very low fat concentrations are of interest for applications to the heart and skeletal muscles. Not only may the fat concentrations expected in the normal condition be very low, the additional accumulation in a disease scenario may be subtle (McGavock *et al.* 2007). Thus for these applications, consideration of estimation precision is especially important. In addition, the feasibility of fat quantification in this range of fat concentrations need to be demonstrated.

The most used application of Water/Fat Imaging-based fat quantification is the measurement of liver fat. This application requires both that images are acquired during breath-hold, and that inhomogeneities of the magnetic field are considered. Both of these challenges may be addressed through the use of a more efficient image acquisition.

The flexible formulation of Water/Fat Imaging methods allow for more complex fat measurements than what has previously been explored. Instead of simple estimation of the fat concentration, it may also be possible to estimate the chemical composition of the accumulated fat. However, it is likely that this extension of Water/Fat Imaging increases the need to carefully consider potential sources of bias.

1.1 Aims

There are three aims of this thesis:

1. To evaluate and optimize methods for fat quantification of low fat concentrations (**Papers I and II**).
2. To develop and evaluate methods for more efficient image acquisition for fat quantification (**Paper III**).
3. To develop and evaluate methods for quantification of the chemical composition of fat (**Papers IV and V**).

2. Human fat and the importance of fat measurements

Fat and obesity have become words of our era, and the growing number and size of obese persons are frequently the subject of media attention. There is, however, much more to the human fat than the numbers on our bathroom scales. This chapter aims at reviewing some background on the healthy and pathological fat in our bodies and motivating why measuring them is of great value in research and diagnostics.
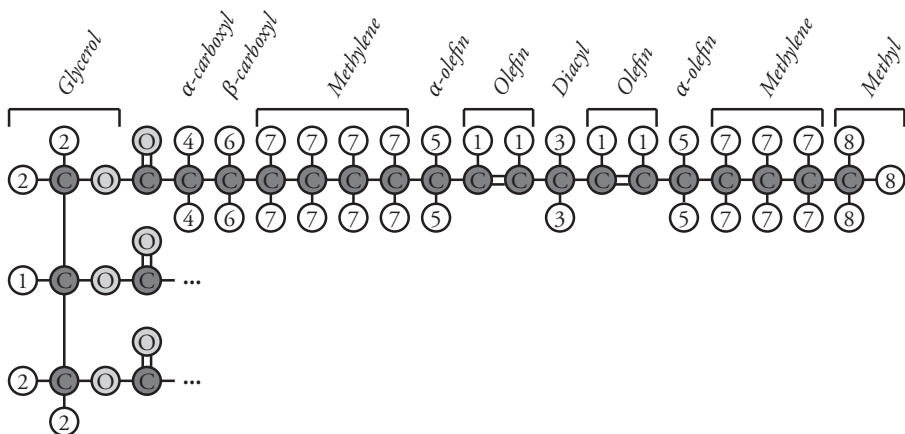
Figure 1. Schematic illustration of a triglyceride molecule showing one out of three fatty acid chains. Carbon atoms are shown in dark grey (C), oxygen atoms in light gray (O), and hydrogen atoms in white. The numbering of hydrogen atoms is consistent throughout this thesis and their respective assignments are of importance for fat signal modeling later on.

2.1 Triglycerides and fatty acid composition

Often, the word fat is used both for the chemical component and for the fatty tissue most of us associate with overweight and obesity. In reality, the word fat refers to triglyceride molecules whereas adipose tissue describes the tissue in which triglycerides are mainly stored in the body. Further, triglycerides are a type of lipid – a group of

molecules including also e.g. cholesterol and phospholipids. Out of the various lipids, triglycerides are the main source of signal in the MR experiment. Phospholipids in the cell membrane have very short spin-spin relaxation time T_2 and will therefore not contribute to the typical MR signal, and cholesterol and free fatty acids give rise to little signal in comparison to triglycerides (Madden *et al.* 1993, Szczepaniak *et al.* 1999).

Triglycerides consist of a glycerol backbone with three fatty acid chains (see Figure 1). Within the body, fat may be stored in adipose tissue or in other organs. Also, a high concentration of fat may be found in bone marrow. Both the length of the fatty acid chain (the number of carbon atoms) and the nature of the bonds between the carbon atoms vary between various fatty acids. Depending on the number of double bonds in the fatty acid chain, they are often described as saturated (no double bonds) or unsaturated (at least one double bond).

2.2 The normal human fat

Most, but not all, triglycerides in the human body are stored in white adipose tissue - a loose connective tissue which is traditionally considered an energy storage depot, a mechanical cushion, and a thermal insulator (ICRP 2002). However, recent research indicates that the white adipose tissue has also a more active role as an endocrine organ and as part of the immune system (Pond 2005, Yang 2008). Most of the fat cell's (adipocyte's) volume consists of a single fat droplet so large that even the cell nucleus is pushed up against the cell membrane. Except for adipocytes, adipose tissue also contain connective tissue, nerves, and blood vessels. Approximately 80 % of the adipose tissue mass consist of fat (ICRP 2002).

Adipose tissue can be found in a number of depots. A suggested classification divides the total adipose tissue into subcutaneous adipose tissue, found just beneath the skin, and internal adipose tissue, found deeper within the body (Shen *et al.* 2003). Both visceral adipose tissue (VAT), found surrounding the internal organs in the abdomen, chest, and pelvis, and intermuscular adipose tissue (IMAT) are examples of internal adipose tissue depots. The IMAT depot is of special interest in **Paper II** and includes adipose tissue located beneath the muscle fascia: either between muscle groups (intermuscular fat), or between muscle cells within the muscle group (intramuscular fat). IMAT should not be confused with intramyocellular lipids (IMCL) which are stored as small fat droplets within the muscle cells. Instead, extramyocellular lipids (EMCL) are defined as lipids stored outside of the muscle cells.

Most fatty acids in human adipose tissue have chain lengths ranging between 14 and 18, and have between zero and two double bonds (Hodson *et al.* 2008). The relative amounts of various fatty acids in adipose tissue are to some extent dependent on the diet (Beynen *et al.* 1980, Hodson *et al.* 2008). However, there are an increasing number

of reports of the fatty acid composition being dependent also on adipose tissue depot, indicating different metabolic activities and thus functions of the various depots (Malcom *et al.* 1989, Lundbom *et al.* 2011, Lundbom *et al.* 2013).

Fat may also be stored within other organs than the adipose tissue, such as the liver, pancreas, or muscles (Snel *et al.* 2012). This type of fat is referred to as ectopic fat and is stored within the organs own parenchymal cells as small droplets within the cell cytoplasm. Normally, the amount of ectopic fat is small and has a function for e.g. cell maintenance (Rasouli *et al.* 2007), or as a source of energy (Schrauwen-Hinderling *et al.* 2006).

2.3 Pathologies and the role of fat measurements

There are several examples of pathological fat accumulation, and in many of them there is a need for various kinds of fat measurements in research and diagnostics. In the following section, the conditions which are the most relevant to this thesis are briefly described.

2.3.1 Obesity and related disease conditions

Obesity is excessive and health-impairing accumulation of fat, and the condition may lead to e.g. insulin resistance, type 2 diabetes mellitus (Snel *et al.* 2012), and cardiovascular disease (Perez Perez *et al.* 2007). Often, the body mass index (BMI), defined as the ratio between the weight [kg] and the squared height [m^2], is used as a measure of overweight and obesity (World Health Organization 2013). However, this measure only relates to the total weight of the person, not to how fat is distributed within the body. Especially the size of the visceral and IMAT depots have been linked to several disease conditions, whereas accumulation of subcutaneous adipose tissue is considered more benign (Perez Perez *et al.* 2007, Rasouli *et al.* 2007). For assessment of the individual volumes of each of these depots, imaging-based methods are required.

In addition to excess adipose tissue, insulin resistance is associated with an increased accumulation of ectopic fat in the liver, pancreas, cardiac muscle, and skeletal muscles; a condition which may lead to organ dysfunction (Rasouli *et al.* 2007, Snel *et al.* 2012). For investigation of ectopic fat accumulation, a quantitative measure of the concentration of fat which can be localized to the specific organ is a crucial step in diagnostics.

The fatty acid composition of accumulated adipose tissue may be associated with insulin resistance (Iggman *et al.* 2010) and inflammatory conditions (Pond 2005). Thus measurements of fatty acid composition may be important in especially research on obesity and related diseases.

2.3.1.1 Hepatic steatosis

A common example of a pathological storage of ectopic fat is hepatic steatosis in which fat is stored in the parenchymal cells of the liver. This condition may be caused by excessive consumption of alcohol, but may also be closely related to obesity and its co-mortalities. In this case, the condition is referred to as NAFLD and may lead to non-alcoholic steatohepatitis (NASH), cirrhosis, and cancer. (Clark *et al.* 2002)

As the fat content is indicative of disease severity, fat measurements are a vital part of diagnostics of this condition. A cut-off of 5.56 % has been suggested to distinguish between normal fat content and hepatic steatosis, but as much as 50 % has been reported in severe cases (Szczepaniak *et al.* 2005). In addition, it has been suggested that measurements of the fatty acid composition may help identify patients in risk of developing the more severe diseases linked to hepatic steatosis (Lee *et al.* 2012, van Werven *et al.* 2012).

2.3.1.2 IMAT accumulation

Excessive accumulation of IMAT is closely related to insulin resistance (Gallagher *et al.* 2005, Boettcher *et al.* 2009), but may also be linked to age (Delmonico *et al.* 2009), inflammation (Beasley *et al.* 2009, Zoico *et al.* 2010), and conditions of chronic pain (Elliott *et al.* 2011, Gerdle *et al.* 2013). Thus, in research on these conditions, a technique which can determine the fat concentration or IMAT volume in skeletal muscle would be valuable.

In muscle the expected fat concentrations range from < 0.5 % and up to 8 %, depending on muscle group (Schick *et al.* 2002). Thus, for measurements of fat accumulation in muscle, the fat measurement technique needs to be sensitive to very low fat concentrations. In addition, the distribution of fat is highly heterogeneous over the muscle compartment, and therefore high resolution imaging would be advantageous.

2.3.2 Lymphedema

Lymphedema is a common, crippling, and painful complication after cancer treatment. Surgical procedures and radiation therapy cause damage to the lymphatic vessels which can no longer transport lymphatic fluid. The result is an accumulation of lymphatic fluid in e.g. an arm or a leg, which can be several liters in volume. (Brorson 2012)

Traditionally, the excess volume is considered to consist of lymphatic fluid only and because of this, bandaging and compression using compression garments have been used for treatment. However, in some cases, these methods have proven ineffective (Brorson 2012). Instead, research has revealed that the excess volume consists mainly of adipose tissue (Brorson *et al.* 2006, Brorson *et al.* 2009), and liposuction with ensuing lifelong compression has become a successful treatment regime (Brorson *et al.*

2006, Brorson 2012). An example of excess adipose tissue in lymphedema is presented in Figure 2.

Preliminary reports show that the condition may also result in an accumulation of intermuscular fat (see **Preliminary reports iv and ix**). This finding may for the first time indicate the presence of lymphedema-induced adipose tissue deposition also beneath the muscle fascia. The close link between lymphedema and an inflammatory condition (Rockson 2013) may also motivate an investigation of the fatty acid composition of the accumulated fat. Thus, fat measurements may be of great value for especially research on lymphedema.
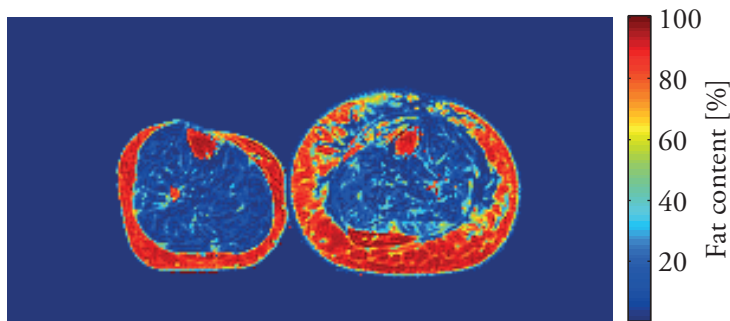
Figure 2. An axial slice through the lower leg of a patient with lymphedema. The color scale represent the fat percentage. The larger size of the patient's left leg is evident, and there is clearly a larger amount of adipose tissue. The image is also a nice example of IMAT accumulation as fatty streaks are evident in the muscle tissue of both legs.

2.4 Summary

The active role of human fat in the normal and pathologic condition is increasingly recognized. Thus, in both research and diagnostics, tools are sought after for identification of fatty areas and quantification of the fat content and the fatty acid composition in various organs and fatty depots. Depending on application, the fat measurement technique may need to provide images, thus facilitating localized measurements and spatial information. In addition, the concentration of fat may need to be quantified on a continuous scale and be sensitive to very low concentrations of fat.

3. Fat measurement techniques and performance analysis

Depending on the application, there are a number of techniques available that, in one way or another, provide a measure of the fat content. It is, however, critically important to keep in mind what it is that each of these techniques actually measure, and what their limitations are. This chapter aims at reviewing and discussing the properties and limitations of existing fat measurement techniques and describing some methods for evaluation of the performance of fat quantification techniques.

3.1 Defining quantitative fat measurements

Fat quantification is used to describe a wide range of fat measurements, all with slightly different goals. There are two main tracks of the fat quantification research area: voxel-by-voxel quantification, and segmented volume quantification. Whereas the former concerns the quantification of a percentage or other quantity on a continuous scale in each image voxel or in a limited area, the latter focuses on quantification of the total volume of a certain area, organ, or tissue. Thus, whereas a voxel-by-voxel fat quantification technique would be able to determine the concentration of fat in e.g. the liver, the segmented volume quantification method would be able to determine the total volume of the VAT depot. Although both are very important, the work presented in this thesis solely concerns voxel-by-voxel fat quantification, and the following discussion will be limited to this track.

For an accurate measurement which may be reliably related to e.g. the fat volume or mass percentage within an organ, the measurement should be *quantitative*. As fat measurements are needed within specific organs, and because fat may be heterogeneously distributed even within a single organ (Hamer *et al.* 2006, Capitan *et al.* 2012), the technique should also provide spatial information. Ideally, the method should thus be based on *tomographic images*. Finally, the method should be *non-invasive* and not use ionizing radiation to make it readily usable for research, for repeated measurements to follow the progression of a disease condition, or to follow up on the effectiveness of a treatment. A summary of the fat quantification techniques reviewed in this chapter and their properties are provided in Table 1.

9

Table 1. Comparison of possible techniques for fat measurements based on desirable properties. For accurate and spatially resolved fat measurements which may be repeated, the ideal technique should be non-invasive, quantitative, based on tomographic images, and not use ionizing radiation. Out of the listed techniques, only the ones based on MR live up to all criteria.

Technique	Non-invasive	Quantitative	Tomographic imaging	No ionizing radiation
Biopsy grading				X
DEXA	X	X		
CT	X		X	
DECT	X	X	X	
US	X		X	X
MRS	X	X	X	X
MRI	X	X	X	X

3.2 Techniques based on non-MRI modalities

3.2.1 Biopsy

Biopsy is traditionally considered the gold standard for diagnosis of ectopic fat accumulation (Clark *et al.* 2002), and is an invasive technique where a small tissue sample is extracted from the organ using a needle. The extracted tissue is graded according to the percentage of cells containing fat droplets, among other visible signs of inflammation and fibrosis (Brunt *et al.* 1999, Kleiner *et al.* 2005). At least for NAFLD applications, the ability of the biopsy technique to distinguish between simple steatosis and inflammation is its main advantage. However, the method is associated with a risk of complications, results only in a course and subjective grading of the disease severity (Brunt *et al.* 1999, Kleiner *et al.* 2005), and suffers from sampling variability as it investigates only a very small fraction of the total liver tissue (Ratziu *et al.* 2005). As a result, it has been suggested that MRI-based techniques may provide a more sensitive measure than biopsy grading, at least for liver applications (Hines *et al.* 2012).

Instead of subjective grading, destructive chemical analysis of the sample may be used to quantitatively estimate the amount of triglycerides in the sample (Hines *et al.* 2012), or the fatty acid composition may be estimated through gas chromatography (Vuppalanchi *et al.* 2007). Although quantitative and useful in research, these methods are not often used in the clinical setting.

3.2.2 X-ray techniques

3.2.2.1 Dual energy X-ray absorption (DEXA)

The different absorptions of two X-ray energies may be used to estimate bone mineral, fat, and lean tissue. The method is widely used and associated with only a very low effective radiation dose (Mattsson and Thomas 2006). However, as it provides 2D planar images only, the possibility to localize the various tissues is limited. The composition of e.g. a limb may be investigated (Brorson *et al.* 2009), but the fat content of the muscle and adipose tissue of the limb may not be measured separately.

3.2.2.2 Computed tomography (CT)

Non-contrast-enhanced computed tomography (CT) is non-invasive and widely available, and its images show decreased attenuation in presence of fatty infiltration of the liver (Schwenzer *et al.* 2009). However, the attenuation is also dependent on e.g. accumulation of glycogen (Leander *et al.* 2000) and iron (Schwenzer *et al.* 2009), which affects the reliability of the technique. In patients, a low diagnostic performance has been demonstrated compared to MR-techniques (van Werven *et al.* 2010). In addition, CT is likely not sensitive for low fat concentrations, and the use of ionizing radiation limits its usefulness in research studies and in follow-up examinations investigating treatment effectiveness.

The difference in attenuation of fatty and lean tissue may also be used for segmentation purposes, and has been used for estimation of e.g. the VAT and IMAT volumes (Beasley *et al.* 2009, Delmonico *et al.* 2009).

3.2.2.3 Dual-energy computed tomography (DECT)

Dual-energy computed tomography (DECT) enables the simultaneous detection of two X-ray energies and tomographic imaging. From the data it is possible to separate the CT signal depending on the various attenuation properties of e.g. fat and water and thus obtain a quantitative measure of their respective amounts (Artz *et al.* 2012). However, a recent study comparing the quantification accuracy of CT and DECT to that of the MRI-based Water/Fat Imaging technique concluded that no gain in accuracy was achieved using DECT compared to CT, and that Water/Fat Imaging demonstrated the superior correlation with fat accumulation (Artz *et al.* 2012).

3.2.3 Ultrasound

The presence of fat droplets in e.g. the liver parenchymal cells increases the echogenicity in ultrasound imaging. Most often, liver steatosis is graded as normal, mild, moderate, or severe based on visual criteria (Strauss *et al.* 2007, Schwenzer *et al.* 2009, Bohte *et al.* 2011). Thus, the assessment of the presence of fatty liver using ultrasound suffers from being operator dependent (Strauss *et al.* 2007), as well as from being insensitive

to small effects on the amount of accumulated fat (Schwenzer *et al.* 2009). In comparison to MR-techniques, a lower diagnostic accuracy has been demonstrated (van Werven *et al.* 2010, Bohte *et al.* 2011).

3.3 MR-based techniques

The MR-based measurement of fat is based on a distinction of the fat signal from signals of other origins (mainly water). Some methods were initially designed to merely suppress the fat signal as it in many applications risks to obscure underlying pathology (Dixon 1984, Haase *et al.* 1985, Meyer *et al.* 1990). Yet others aim at identifying the fat and water signals for fat depot segmentation purposes (Staten *et al.* 1989, Abate *et al.* 1994, Schick *et al.* 2002, Machann *et al.* 2005). Some of these techniques may, however, be altered or complemented to allow for quantitative voxel-by-voxel fat measurements. The estimation of a truly quantitative measure may be reliant on the homogeneities of the main magnetic field (B_0) and the radio-frequency (RF) pulse field (B_1), in addition to contrast weighting.

For distinction of the fat signal from that of others, some property of the fat signal needs to be unique. In the following section, the properties of the fat MR signal are reviewed before some examples of MR-based fat measurements are briefly described.

3.3.1 Fat as seen in MR

It is commonly known that the fat and water relaxation times differ. Especially, the spin-lattice relaxation time T_1 of fat is shorter than that of water, and the difference is especially large in muscle tissue. Some typical relaxation values of fat and water are summarized in Table 2.

Table 2. Relaxation times of water and fat (methylene) in three tissues as reported at 3 T. Values were obtained from [a](Hamilton, Smith*, et al.* 2011), [b](Hamilton *et al.* 2013), and [c](Krssak *et al.* 2004).

	T_1 (ms)		T_2 (ms)	
	Water	Fat	Water	Fat
Subcutaneous adipose tissue[a]	1053	280	21.7	54.7
Liver[b]	933	361	25.9	53.6
Soleus muscle (EMCL)[c]	1377	369	31.3	77.6

Due to electron shielding of the magnetic field, the field experienced by a proton differs slightly depending on its chemical environment (Knight 1949). This effect is known as the chemical shift, and causes different resonance frequencies of protons in different molecules, but also of protons at different position within the same molecule. The size

12

of the shift is linearly dependent on the external magnetic field and is often expressed in ppm relative to this field (Stark and Bradley 1992). The phenomenon is known to cause the notorious chemical-shift artifact where the signal of fat is offset spatially from the signal of water in the read-out direction. However, it is also the effect behind the MR spectroscopy technique and several other MR-based fat measurement techniques. An example oil spectrum is provided in Figure 3 and each of the visible fat peaks is attributable to one of the chemical groups of the triglyceride molecule as summarized in Table 3 and illustrated in Figure 1.

Table 3. Peak assignment of the individual fat resonances (see also Figure 1 and Figure 3).

Peak number	Chemical shift (ppm)[a]	Assignment	Chemical group
1	5.29	-**CH**=**CH**-	Olefin
	5.19	-**CH**-O-CO-	Glycerol
2	4.20	-C**H₂**-O-CO	Glycerol
3	2.75	-CH=CH-C**H₂**-CH=CH-	Diacyl
4	2.24	-CH₂-C**H₂**-COO	α-carboxyl
5	2.02	-C**H₂**-CH=CH-	α-olefin
6	1.60	-C**H₂**-CH₂-COO	β-carboxyl
7	1.30	-(C**H₂**)$_n$-	Methylene
8	0.90	-CH₂-C**H₃**	Methyl

[a] As observed in the liver by Hamilton *et al.* (Hamilton, Yokoo, *et al.* 2011)

As is evident from Figure 3, the methylene signal is six times more intense than that of any other fat peak. However, its signal only corresponds to roughly 70 % of the total fat signal (Hamilton, Yokoo, *et al.* 2011). The chemical shift between the dominant fat peak, methylene (peak 7), and water is approximately -3.4 ppm *in vivo* corresponding to approximately -220 Hz at 1.5 T and -440 Hz at 3 T. Although the chemical shifts between the various fat resonances are constant, the fat/water chemical shift is dependent both on temperature (Kuroda *et al.* 1997) and on bulk susceptibility effects (Szczepaniak *et al.* 2002).

Temperature affects the chemical shift of water much more than that of fat, causing a temperature dependent frequency difference between the two. In room temperature, the shift between water and methylene is approximately -3.53 ppm (**Paper I**), compared to -3.4 ppm *in vivo* (Hamilton, Yokoo, *et al.* 2011). This is not often a concern for *in vivo* imaging, but may be important to consider for *in vitro* and phantom experiments (Hernando *et al.* 2013).

Bulk susceptibility effects cause the magnetic field experienced by fat protons to depend on the way fat is stored. In case of small fatty droplets in the cell cytoplasm or in fat/water emulsions, the fat/water shift is constant. In case of fat stored in adipocytes between other types of cells, such as muscle fiber bundles, the fat/water shift becomes

dependent on the angle of the fiber bundles to the external magnetic field. The additional shift caused by this effect is up to 0.2 ppm depending on orientation of the fiber bundles (Szczepaniak *et al.* 2002). Thus, the bulk susceptibility effect is not likely of concern in case of measurements in emulsions or ectopic fat, but may be important to consider in case of measurements of intermuscular fat as the angle of the muscle fibers are different in different muscle groups (Karampinos, Yu, *et al.* 2012).
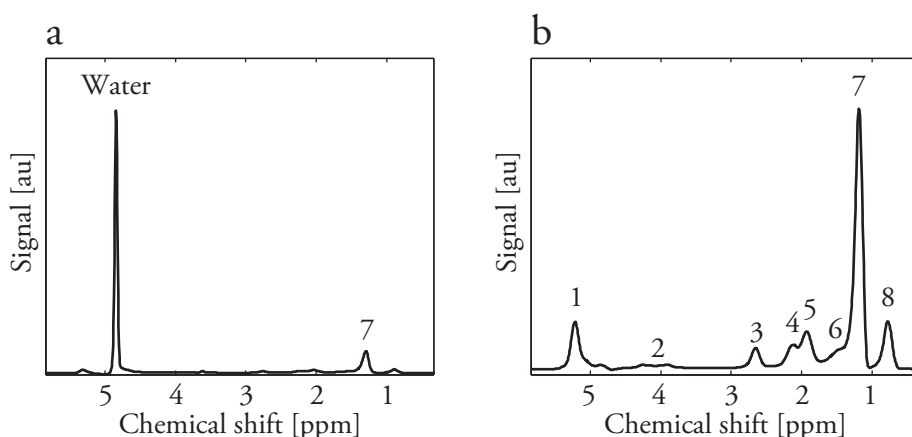

Figure 3. MR spectra from Intralipid with 20 % fat concentration (a) and pure soybean oil (b) acquired at 3 T. Numbers indicate peak assignments as further described in Table 3. In a) only water and the dominant fat peak (peak 7) are assigned, whereas eigth fat peaks are assigned in b).

3.3.2 Magnetic resonance spectroscopy (MRS)

^{1}H-MRS is considered the gold standard of non-invasive fat quantification methods. Most often, a single voxel is excited using either a stimulated echo acquisition mode (STEAM) (Frahm *et al.* 1987) or a point-resolved spectroscopy (PRESS) localization technique (Bottomley 1987) after which the signal is sampled and Fourier transformed. From the information acquired, curve-fitting to either the signal or spectrum is used to estimate the intensity of the individual spectral components.

MRS has demonstrated excellent diagnostic performance for e.g. liver applications (Roldan-Valadez *et al.* 2010, Bohte *et al.* 2011, Kang *et al.* 2012). In addition, the technique makes it possible to also estimate the chemical composition of fat as individual fat peaks may be estimated (Guillén and Ruiz 2003, Hamilton, Yokoo, *et al.* 2011, Lundbom *et al.* 2011, van Werven *et al.* 2012). The technique may also be used to distinguish between IMCL and EMCL in muscle tissue (Boesch *et al.* 1997), which is currently not possible using any imaging-based techniques. However, measurements are limited to an approximately 10-ml volume and does not provide additional spatial information. MRS also require analysis by an experienced observer.

To obtain also spatial information from the MRS experiment, it is possible to phase encode the signal in two or even three dimensions (Maudsley *et al.* 1983). The technique offers detailed spectral information in each voxel, and has been used for e.g. quantification of IMCL (Hwang *et al.* 2001). However, the spatial resolution is often still lower than that of imaging methods and the technique is associated with a lengthy acquisition time.

3.3.3 Magnetic resonance imaging (MRI)

3.3.3.1 T_1-weighted imaging

Due to its shorter T_1 time, fat appears bright on T_1-weighted images, a feature often considered a nuisance. The effect has been used mainly for segmentation of fat signal (Staten *et al.* 1989, Abate *et al.* 1994, Gallagher *et al.* 2005, Machann *et al.* 2005, Boettcher *et al.* 2009), but is not quantitative on a voxel-by-voxel basis, or sensitive to lower fat concentrations.

3.3.3.2 Fat-selective imaging

Using the frequency difference between water and fat, a frequency-selective RF pulse may be used to excite a spectral band of fat protons only (Meyer *et al.* 1990, Schick *et al.* 2002). However, as the frequency band corresponding to the fat signal is dependent on the magnetic field, the technique is sensitive to B_0-inhomogeneities. In addition, the approach require correction of B_1-inhomogeneities as well as calibration against a pure fat reference if it is to be used for quantitative fat measurements.

3.3.3.3 Fat suppressed/Non-fat suppressed imaging

The chemical shift of fat relative to water may also be used to suppress the fat signals using frequency-selective saturation pulses and crusher gradients in preparation of signal excitation, leaving very little fat signal to excite (Haase *et al.* 1985). Although this approach is often used for fat suppression only, complementary acquisition of a separate, non-fat-suppressed image, allow for fat measurements (Bernard *et al.* 2008, Reeder *et al.* 2011). Although B_1-inhomogeneities should be cancelled in the estimation of the fat-suppressed/non-fat-suppressed ratio, the efficiency of the fat suppression is sensitive to B_0-inhomogeneities. In addition, the fat suppression cannot suppress fat signals close in frequency to the water peak, such as the olefinic peak (peak 1), which will bias the estimated fat measure.

3.3.3.4 Water/Fat Imaging

Chemical-shift-encoding techniques, or Water/Fat Imaging techniques, are also based on the chemical shift of the fat signal. Instead of suppressing or exciting one of the fat or water signals, a post-processing algorithm is used to sort the signals into separate fat and water images, respectively. This approach can be made robust against both B_0- and

B$_1$-inhomogeneities and provides fat quantification on a continuous scale which is sensitive to a wide range of fat concentrations (Reeder *et al.* 2011), even the very low concentrations expected in muscle tissue (**Paper I**).

Quantification of fat using Water/Fat Imaging may be viewed as a three-step process where the first is image acquisition, and the second two are both part of post-processing (see Figure 4):

1. *Image acquisition* (Chapter 4)
2. *Separation* of signals using signal modeling (Chapter 5)
3. *Quantification* (Chapter 6)

1. Image acquisition

2. Separation

Water   Fat

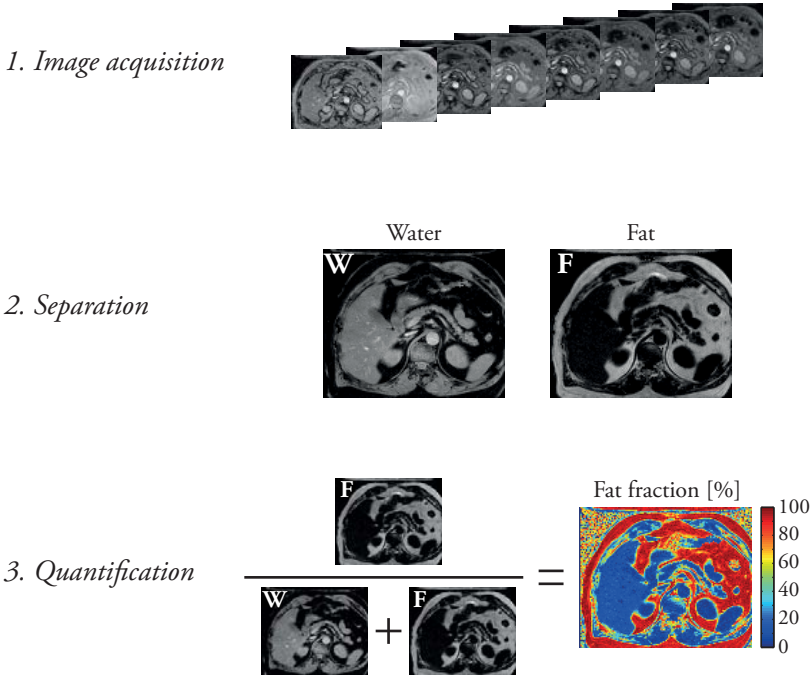

3. Quantification

Fat fraction [%]

Figure 4. Schematic illustration of the three steps of the Water/Fat Imaging technique: 1. *Image acquisition* in which a number of images with various echo times are acquired; 2. *Separation* in which the signals are sorted into images representing each of the signal species; and 3. *Quantification* in which the fat fraction, a quantitative measure of the fat concentration, is calculated. An axial slice over the liver of a patient subject is used as an example.

The key aspect of Water/Fat Imaging is the signal evolution over echo time which results from the chemical shift between the water and fat signals, referred to as ρ_w and ρ_f, respectively. This aspect is illustrated in Figure 5. Due to the different frequencies of the two signal components, the total signal intensity oscillates between their in-phase and opposed-phase positions. By sampling this evolution in image acquisition and modeling it in post-processing, the intensity of the two signal species may be estimated.

In the quantification step, the fat fraction FF is estimated from the two separated images:

$$FF = \frac{\rho_f}{\rho_f + \rho_w} \tag{3.1}$$

Alternatively, e.g. the number of double bonds (-CH=CH-) of the triglyceride molecule may be quantified as a measure of the fatty acid composition using the same basic steps.
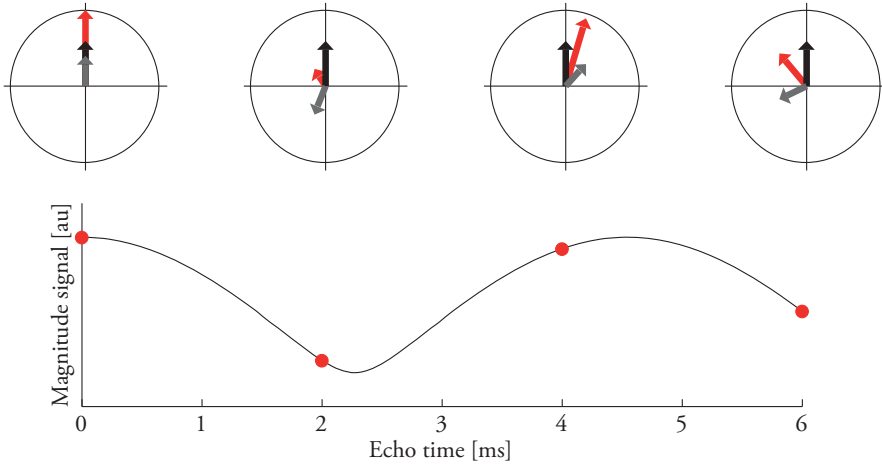
Figure 5. Schematic illustration of the signal evolution due to the chemical shift between water and fat. Phase diagrams illustrate the magnetization vectors of the water (black), fat (gray), and the total signal (red) at the echo times acquired (red dots).

3.4 Methods for performance evaluation

For evaluation of the performance of the various techniques investigated, simulations, phantom experiments, and *in vivo* comparisons were conducted in this thesis. Whereas simulations make it possible to isolate a specific effect, the *in vivo* application is of course the ultimate goal. Phantom experiments are a valuable intermediate step where a range of controlled FFs or fatty acid compositions may be imaged simultaneously.

3.4.1 Phantom construction

Preferably, both the fat concentration and the fatty acid composition of phantoms should be adjustable and well known, and the T_1 and T_2 values of the signal components should be relevant for *in vivo* conditions. Pure fat phantoms are easily obtained using vegetable oils whose fatty acid composition may be obtained from the manufacturer or gas chromatography measurements.

A reasonable model of ectopic fat and intermediate FFs is a fat/water emulsion. Intralipid (Fresenius Kabi, Sweden) was used in **Papers I, II, III,** and **IV** and is a stable emulsion of soybean oil in a salt solution with FF = 20 % which may be diluted with purified water to the desired fat concentration. There are mainly three disadvantages of Intralipid for fat/water phantom purposes: The limited fat concentration of only 20 %, the presence of the emulsifying agent lecithin which is an MR-visible lipid, and the single fatty acid composition available.

Instead, it is possible to construct fat/water emulsions from scratch by fixating fat/water emulsions using agarose, thus creating fat/water gels with adjustable water T_2 as was done in **Paper IV** (Bernard *et al.* 2008, Hines *et al.* 2009). Sodium dodecyl sulfate may be used as an emulsifying agent in sufficiently low concentration not to interfere with the MR signal. The main advantage of this approach is the possibility to control both the fat concentration and the fatty acid composition by changing the oil used. However, fat concentrations higher than approximately 50 % are very difficult to achieve and the manufacturing process is rather time consuming.

The range of FFs achievable using Intralipid or fat/water gels are both relevant for measurements of e.g. hepatic steatosis (Szczepaniak *et al.* 2005) and in both cases, low FFs may be constructed (**Papers I and II**). In addition, the T_1 of the water phase may be adjusted using a contrast agent or nickel salt.

3.4.2 Measures of performance

A number of measures are used in the evaluation of the performance of a method. This section aim at reviewing those used in the papers of this thesis, and should not be regarded a complete description of methods available.

3.4.2.1 Accuracy

Accuracy of the various techniques have in this thesis been investigated using regression analysis (slope and intercept), Bland-Altman analysis (bias and limits of agreement), and standard deviation from the true value SD_{ftv} defined as:

$$SD_{ftv} = \sqrt{\sum_{i=1}^{I} \frac{\left(\rho_i - \rho_{known,i}\right)^2}{I}} \qquad (3.2)$$

In this expression, I denotes the number of measurements, ρ the estimated parameter and ρ_{known} the true value. Each measure has its own respective advantage and disadvantage. A Bland-Altman analysis is recommended for comparisons between different measurement techniques (Altman and Bland 1983). For comparison against known values, a regression analysis is often the most illustrative. However, in these cases the SD_{ftv} may provide a complementary measure which is more directly associated with the actual agreement with known values compared to the slope and intercept.

3.4.2.2 Precision

The precision of the estimated parameters is most often shown as the standard deviation. However, the standard deviation within a region-of-interest in phantoms or *in vivo* is not only a measure of the estimation precision, but also reflects the presence of artifacts or anatomical variance. For comparison of various methods, at least the anatomical variance should be identical and the standard deviation may be a relevant measure of precision in methods comparison.

3.4.2.3 Noise performance

The Gaussian noise in an MR image is often measured in terms of the signal-to-noise ratio (SNR). However, in the case of separation of the fat and water signals, a number of MR images are acquired and used in calculations. A useful measure of how the noise in each of these images propagates through the estimation process is the effective number of signal averages NSA, defined as (Glover 1991):

$$NSA = \frac{\sigma_\rho^2}{\sigma_S^2} \qquad (3.3)$$

where σ_ρ^2 is the variance of the estimated parameter ρ (e.g. the fat or water signal) and σ_S^2 is the variance in one of the raw data signals. Thus, the maximum NSA correspond to the situation where the signal originate from only one signal species and is obtained as an average of the N images acquired. In this case, the NSA is equal to N.

NSA may be either computed from simulated signals with added Gaussian noise (see **Paper IV**), or analytically calculated from the signal model (see **Paper III**). Alternatively, a number of repeated image acquisitions may be performed and the NSA estimated from the variance of the repeated raw data images and of the repeated estimations of ρ (see **Paper III**).

Using an analytical approach, NSA may be estimated from the Cramér-Rao Bound (CRB) (Pineda *et al.* 2005). The CRB is the lowest possible variance of an estimate ρ and may be calculated using the following formula, where $*$ denotes the complex conjugate and S_n the nth signal out of a total of N (Scharf and McWhorter 1993):

$$CRB_\rho \geq \frac{1}{\frac{2}{\sigma_S^2} \Sigma_{n=1}^{N} Re\left[\left(\frac{\partial S_n}{\partial \rho}\right)^* \left(\frac{\partial S_n}{\partial \rho}\right)\right]} \tag{3.4}$$

3.4.2.4 Repeatability

The repeatability of a method is an important measure and may be used in the determination of how small differences in FF or fatty acid composition that may be distinguished using the method tested. Using a Bland-Altman analysis of the repeated measurements, the bias should be zero and the 95 % limits of agreement (or the coefficient of repeatability) indicates in what range 95 % of repeated measurements will fall (Altman and Bland 1983).

3.5 Summary

MRI is the only diagnostic tool available in the hospital that has the potential for non-invasive and quantitative fat imaging. Out of the methods available using MR-techniques, Water/Fat Imaging is the most promising as it allows for quantitative measurements in a wide range of fat concentrations which can be made robust against several confounding factors. For evaluation of method performance (accuracy, precision, repeatability, and noise performance), simulations, phantom experiments, and *in vivo* investigations have been conducted in this study.

4. Image acquisition

In the world of MR, there is unfortunately no such thing as a simple "Go" button. Instead, there is a wide variety of pulse sequences and imaging parameters which need to be chosen and optimized for each image acquisition. What is basically needed in terms of raw data in Water/Fat Imaging, are a number of images which sample the signal evolution due to the chemical shift of fat and water. The aim of this chapter is to review the various ways in which this may be accomplished and to discuss imaging parameters which are of importance for Water/Fat Imaging. In particular, the use of a more efficient sampling scheme for fat quantification and acquisition of data for estimation of fatty acid composition have been investigated in this thesis.

4.1 Pulse sequence

There are several alternative pulse sequences and acquisition schemes available for the acquisition of the images needed for separation of fat and water signals. Although the first few works suggesting Water/Fat Imaging techniques were all based on spin-echo sequences with slightly asymmetrically timed 180° pulses (Dixon 1984, Sepponen *et al.* 1984, Blatter *et al.* 1985), most techniques now rely on gradient-echo sequences (Reeder *et al.* 2007). Separation of fat and water signals has also been presented from gradient- and spin echo (GRASE) (Li *et al.* 2007) and balanced steady-state free precession (bSSFP) images (Leupold *et al.* 2006). In this thesis, gradient-echo images were used exclusively, and therefore, the following discussion on image acquisition is limited to the use of gradient-echo images.

Naturally, each of the multiple echoes may be acquired as separate scans, but such an approach increases risk for misregistration between images and is unnecessarily time consuming. Much more efficient is the option of acquiring all desired echoes in a single sequence during one repetition time (TR). Most often, this is achieved using unipolar gradients where the data acquisition is paused during fly-back gradients (see Figure 6a). Instead, the image acquisition may be made even more efficient using bipolar read-out gradients where also the gradient of opposed polarity are used for signal acquisition (see Figure 6b). However, artifacts associated with a bipolar acquisition call for careful consideration in fat quantification as investigated in **Paper III** and described in Chapter 0.

Additional methods of reducing the imaging time are parallel imaging and compressed sensing techniques. Whereas parallel imaging is frequently used in Water/Fat Imaging, compressed sensing for this application has not until recently been developed and may be a promising new tool to make image acquisition more effective (Doneva *et al.* 2010).
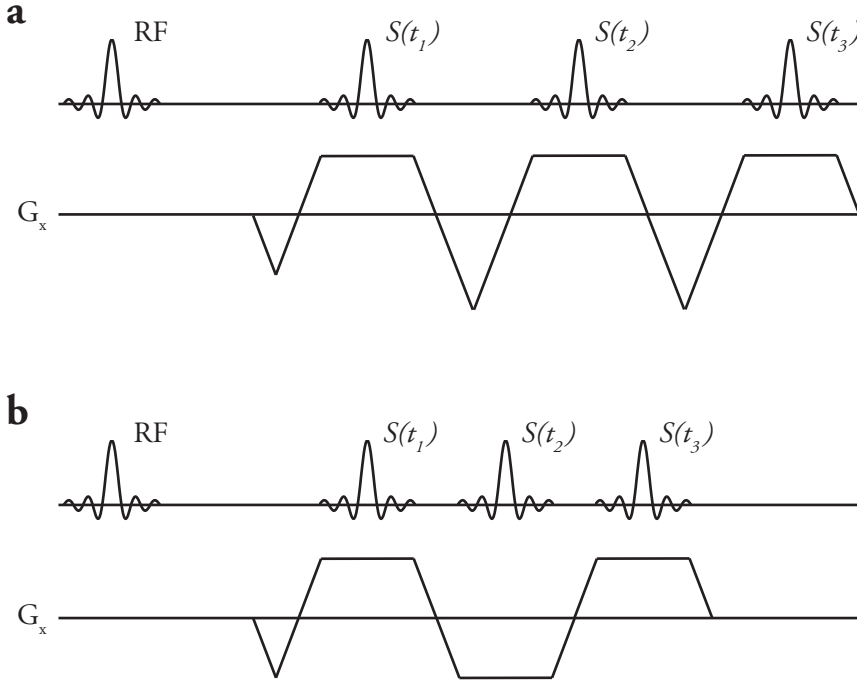

Figure 6. Schematic illustration of pulse sequences with unipolar (a) and bipolar gradients (b), respectively. Only the read-out gradient G_x is included in the illustration.

4.2 Imaging parameters

For all MRI techniques, the choice of imaging parameters is a balancing act between time, resolution, and SNR. For the noise performance of fat/water separation, the number of echoes and the time difference between them are important parameters, whereas TR and flip angle are important to consider for accurate and precise fat quantification (see Chapter 6.2). For a general discussion on sampling scheme which is independent of field strength, the inter-echo time Δt is usually expressed in terms of inter-echo shift, i.e. the phase difference between the magnetization vectors of water and the dominant fat peak.
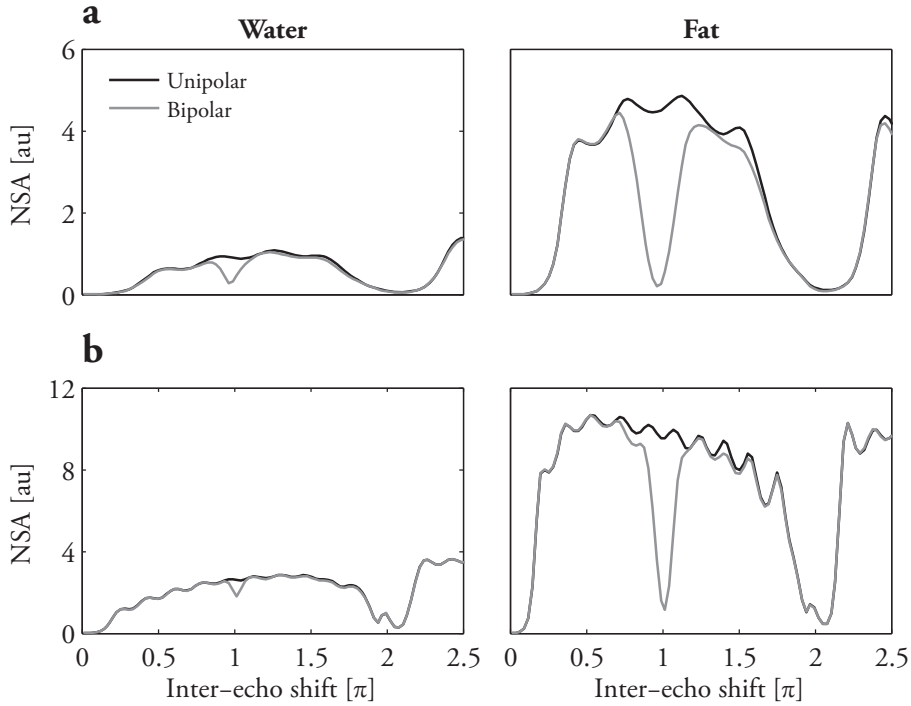
Figure 7. Theoretically estimated NSAs of the decomposed water (left column) and fat (right column) from six (a) and twelve (b) echoes in 30 % fat concentration. Estimation was conducted both for a separation assuming a unipolar acquisition scheme (black), and a separation correcting for a bipolar acquisition scheme (gray). (Paper III)

Early in the development of Water/Fat Imaging techniques only two or three echoes were acquired (Dixon 1984, Blatter *et al.* 1985, Lodes *et al.* 1989, Glover 1991), and effort was put into the selection of the inter-echo shifts which resulted in the optimal noise performance (Glover 1991, Pineda *et al.* 2005, Reeder *et al.* 2007). As the number of echoes grew, the noise performance became less dependent on the exact sampling scheme, and instead Δt may be chosen to the shortest possible (Yu, McKenzie*, et al.* 2007). Especially, minimizing the first echo time has a large impact on the noise performance of the method (Reeder *et al.* 2012). However, a choice of a 2π inter-echo shift should always be avoided (see Figure 7).

In **Paper III**, the shortest possible Δt was decreased using a bipolar acquisition scheme, potentially leading to a number of benefits. First, a shorter Δt makes the acquisition less sensitive to the effective transverse relaxation T_2^* and makes possible the reduction of TR and the total scan time. A shorter scan time makes the acquisition less sensitive to motion artifacts as well as more compatible with breath-hold imaging, an important property in abdominal applications. Second, the range of off-resonance frequencies that

may be resolved increases with decreasing Δt (Yu, Shimakawa, *et al.* 2007). Third, a reduced Δt allows for a closer sampling of the fat/water phase evolution, which makes the water/fat separation process less sensitive to model inaccuracies (**Paper I**). Both the second and third points are especially important to consider, as the MR community currently tends to move towards the use of higher and higher field strengths, making shimming more challenging and increasing the fat/water frequency shift.

The optimal sampling scheme from a noise performance point-of-view may be different for the unipolar and bipolar acquisition schemes, and for that reason, the NSAs of the two approaches were compared in **Paper III** (see Figure 7). The results demonstrate similar NSAs for most inter-echo shifts, but a choice of a π inter-echo shift was found to be suboptimal in case of a bipolar acquisition scheme. However, the sensitivity to the inter-echo shift was reduced by an increased number of echoes.

The noise performance as a function of Δt was investigated for quantification of the fatty acid composition in **Paper IV** (see Figure 8). In comparison to fat quantification, the choice of Δt was more delicate due to the interference of several frequency components. For this application, also the total sampling time may be of interest as it controls the spectral resolution (Berglund *et al.* 2012). A similar result was found in **Paper V**, where a sampling time shorter than approximately 10 ms did not provide a stable estimation at 3 T.
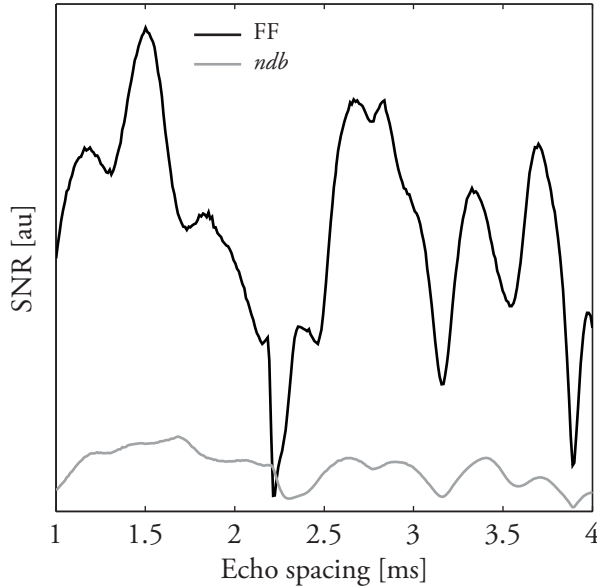

Figure 8. Simulated SNRs of the estimated FF and the fatty acid composition parameter *ndb* (number of double bonds) as function of inter-echo time using eight echoes. The noise performance of estimation of fatty acid composition is more dependent on the inter-echo time than simple fat/water separation. (Paper IV)

4.3 Summary

The acquisition of the images needed for Water/Fat Imaging may be achieved from a standard multi-gradient-echo sequence available at the typical clinical scanner. The acquisition of all echoes in a single TR is recommended as well as a flexible, multi-point acquisition given that a 2π inter-echo shift is avoided. From the results of this thesis, it may also be recommended to choose the shortest possible Δt (**Paper I**). In addition, the shortest possible Δt may be decreased using a bipolar acquisition scheme (given appropriate correction of associated errors) (**Paper III**). However, both for the use of a bipolar acquisition scheme and for the estimation of fatty acid composition, some care is necessary to avoid a sampling scheme associated with a suboptimal noise performance (**Papers III, IV, and V**).

5. Separation using signal modeling

Thanks to the imaging of hydrogen protons, the MR technique is especially suited to analyze the contents of fat and water, two of the most abundant components of the human body. Using modeling of the chemical shift between the two, it is possible to "sort" the MR signal into separate fat and water images. In this section, various signal models used for separation of fat and water are reviewed and their performance discussed for different applications. Especially, methods for modeling T_2 differences, correction of the errors associated with a bipolar acquisition, and mapping of the fatty acid composition are developed and investigated in this thesis.

5.1 Fixed 2- and 3-point techniques

The field of fat/water separation began with the 2-point technique suggested by Dixon in 1984 (Dixon 1984). This simple approach considers only the presence of a water and a single fat resonance in each voxel with position (x,y). In this approach, two images are acquired with two echo times (two points) adapted to yield the in- and opposed-phase positions of the fat and water signals, respectively:

$$S_{IP}(x, y) = \rho_w(x, y) + \rho_f(x, y)$$
$$S_{OP}(x, y) = \rho_w(x, y) - \rho_f(x, y)$$

(5.1)

The in- and opposed-phase images are referred to as S_{IP} and S_{OP}, respectively. Thanks to the well-thought-out acquisition, ρ_w and ρ_f may be calculated using simple addition and subtraction of the two images.

Unfortunately, the technique is sensitive to the presence of an inhomogeneous B_0 field which causes the fat and water signals to deviate from the expected phase positions. To simultaneously estimate the B_0-field inhomogeneities and the water and fat signals, 3-point methods were introduced which allowed additional information to be estimated from the data (Lodes *et al.* 1989, Glover 1991). For these methods, various fixed sampling schemes (fixed number of echoes with fixed inter-echo shifts) were used to allow an analytical solution of the three unknowns.

5.2 Generalized multi-point techniques

Instead of requiring a fixed sampling scheme, a generalized approach was suggested where any number of complex-valued echoes N with arbitrary echo times may be used (Reeder *et al.* 2004). In addition, an arbitrary number of signal components P may be decomposed. This approach has been the foundation of the papers presented in this thesis and it will therefore be described in some detail.

The original point of the technique was an iterative estimation of the off-resonance frequency ψ [Hz]. For the case of fat/water separation (P=2), with Δf [Hz] denoting the chemical shift of fat relative to water, the generalized signal expression at the nth echo time t_n [s] becomes:

$$S(x,y,t_n) = [\rho_w(x,y) + \rho_f(x,y)e^{i2\pi\Delta f t_n}]e^{i2\pi\psi(x,y)t_n} \tag{5.2}$$

The signal expression may alternatively be expressed in matrix form, where $\boldsymbol{\rho}_{Px1}$ represent the intensity of the P signal components to be decomposed, $\mathbf{A}_{NxP}$ contain *a priori* information on the signal evolution due to chemical shift and, possibly, relaxation (see Chapter 5.3), $\mathbf{D}_{NxN}$ contain off-resonance effects and $\mathbf{S}_{Nx1}$ contain the signals acquired. The matrices corresponding to eq. 5.2 become:

$$\boldsymbol{\rho}_{2x1} = \begin{bmatrix} \rho_w(x,y) \\ \rho_f(x,y) \end{bmatrix} \tag{5.3}$$

$$\mathbf{A}_{Nx2} = \begin{bmatrix} 1 & e^{i2\pi\Delta f t_1} \\ 1 & e^{i2\pi\Delta f t_2} \\ \vdots & \vdots \\ 1 & e^{i2\pi\Delta f t_N} \end{bmatrix} \tag{5.4}$$

$$\mathbf{D}_{NxN} = \begin{bmatrix} e^{i2\pi\psi(x,y)t_1} & 0 & \cdots & 0 \\ 0 & e^{i2\pi\psi(x,y)t_2} & \cdots & 0 \\ \vdots & \vdots & \ddots & \vdots \\ 0 & 0 & \cdots & e^{i2\pi\psi(x,y)t_N} \end{bmatrix} \tag{5.5}$$

Each of these matrices may be altered in order to extend or adjust the signal model chosen. A number of commonly used signal models are described in the following sections. The signal equation thus becomes:

$$\mathbf{S} = \mathbf{DA\rho} \tag{5.6}$$

Given that the matrix $\mathbf{D}$ is known, an estimate of the matrix $\boldsymbol{\rho}$ (denoted $\widetilde{\boldsymbol{\rho}}$) may be obtained using a least-squares estimation:

$$\widetilde{\boldsymbol{\rho}} = (\mathbf{A}^T\mathbf{A})^{-1}\mathbf{A}^T\mathbf{D}^{-1}\mathbf{S} \tag{5.7}$$

However, as this is not often the case, an iterative procedure has been suggested which estimates also ψ (and thus $\mathbf{D}$) in the decomposition process. The procedure is based on a linearization of the estimation problem. Starting from eq. 5.2, a Taylor expansion results in the following expression:

$$S(x,y,t_n) = [\rho_w(x,y) + \rho_f(x,y)e^{i2\pi\Delta f t_n}](1 - i2\pi\psi(x,y)t_n) \tag{5.8}$$

By defining a matrix $\mathbf{B}_{NxP+1}$, approximate estimations of the errors of $\tilde{\rho}_w$, $\tilde{\rho}_f$, and $\tilde{\psi}$ denoted $\Delta\tilde{\rho}_w$, $\Delta\tilde{\rho}_f$, and $\Delta\tilde{\psi}$, respectively, may be obtained according to:

$$\begin{bmatrix} \Delta\tilde{\rho}_w(x,y) \\ \Delta\tilde{\rho}_f(x,y) \\ \Delta\tilde{\psi}(x,y) \end{bmatrix} = (\mathbf{B}^T\mathbf{B})^{-1}\mathbf{B}^T(\mathbf{D}^{-1}\mathbf{S} - \mathbf{A}\widetilde{\boldsymbol{\rho}}) \tag{5.9}$$

where

$$\mathbf{B} = \begin{bmatrix} 1 & e^{i2\pi\Delta f t_1} & \left(\tilde{\rho}_w(x,y) + \tilde{\rho}_f(x,y)e^{i2\pi\Delta f t_1}\right)i2\pi t_1 \\ 1 & e^{i2\pi\Delta f t_2} & \left(\tilde{\rho}_w(x,y) + \tilde{\rho}_f(x,y)e^{i2\pi\Delta f t_2}\right)i2\pi t_2 \\ \vdots & \vdots & \vdots \\ 1 & e^{i2\pi\Delta f t_N} & \left(\tilde{\rho}_w(x,y) + \tilde{\rho}_f(x,y)e^{i2\pi\Delta f t_N}\right)i2\pi t_N \end{bmatrix}. \tag{5.10}$$

Note that the first two columns of the matrix $\mathbf{B}$ are identical to the matrix $\mathbf{A}$. Using these expressions, a step-by-step algorithm may be used to iteratively fine-tune the estimates $\tilde{\rho}_w$, $\tilde{\rho}_f$, and $\tilde{\psi}$:

1. Start from an initial guess of the parameters $\tilde{\rho}_w$, $\tilde{\rho}_f$, and $\tilde{\psi}$.
2. Using the current estimate of $\tilde{\psi}$, use eq. 5.7 to obtain a new estimate of the parameters $\tilde{\rho}_w$ and $\tilde{\rho}_f$.
3. Using the current estimates of $\tilde{\rho}_w$, $\tilde{\rho}_f$, and $\tilde{\psi}$, use eq. 5.9 to obtain a new estimate of $\Delta\tilde{\psi}$.
4. Update the estimated $\tilde{\psi}$ using $\tilde{\psi} = \tilde{\psi} + \Delta\tilde{\psi}$.
5. Repeat steps 2-3 until $\Delta\tilde{\psi}$ is smaller than a predefined criterion or until a maximum number of iterations is reached.

5.2.1 Formulation based on magnitude signals

Instead of estimating the off-resonance frequency, the separation may be made insensitive to an inhomogeneous field and phase errors by the use of magnitude instead of complex raw data. Separation from magnitude images does require a modified iterative algorithm in case of a flexible sampling scheme (Yu *et al.* 2011), but is easily combined with the algorithm described above in case of a fixed in- and opposed-phase approach.

Using magnitude data, it is possible to separate the dominant from the non-dominant signal species only; for correct assignment of fat and water, phase information is needed. Thus, 0 % - 50 % fat concentrations may be correctly assigned, a range which may be sufficient for e.g. liver applications (Szczepaniak *et al.* 2005). It is also important to note that the noise performance of the magnitude approach is lower than that using complex-valued data (Hernando, Liang, *et al.* 2010). Therefore, hybrid approaches have been suggested which utilize both the superior noise performance of a complex reconstruction and the insensitivity to phase errors of magnitude data (Yu *et al.* 2011, Hernando *et al.* 2012).

In **Paper I**, the accuracies of magnitude and complex in- and opposed-phased data for fat quantification were compared and the magnitude approach was found to result in lower accuracy than the use of a complex approach. This result is likely due to inaccuracies of the in- and opposed-phase positions because of the multi-peak fat spectrum. The finding is consistent with the higher sensitivity of the magnitude reconstruction to model inaccuracies found in other studies (Hernando, Liang, *et al.* 2010, Hernando *et al.* 2013).

5.2.2 Avoiding fat/water swaps

There are two aspects of the field inhomogeneity problem: A correct estimation of the off-resonance frequency on a continuous scale and the correct assignment of the fat and water signals. The iterative procedure described above addresses the first of these, but even with this approach, so called fat/water swaps must be considered. A fat/water swap

occurs in cases where either the fat or the water signal is erroneously assigned as the other signal component. An intuitive example is a pure fat voxel with 3.4 ppm off-resonance frequency. The signal from this voxel may just as well be described by a pure water signal with 0 ppm off-resonance, as the frequency of the off-set fat signal is in this case identical to that of an on-resonance water frequency.

Most techniques suggested to handle this issue uses an assumption that the off-resonance-frequency map should be smooth, i.e. that there should be no sudden large changes of the off-resonance frequency over the image. This assumption has been implemented through e.g. region-growing (Xiang and An 1997, Ma 2004, Yu *et al.* 2005, Berglund *et al.* 2010) and graph-cut techniques (Hernando, Kellman*, et al.* 2010, Berglund and Kullberg 2012).

5.3 Inclusion of T_2^*-dephasing

Signal dephasing due to T_2^* [s] has an impact on the signal evolution over echo time and depend on the intrinsic T_2 [s] dephasing and the extrinsic T_2' [s] which is governed by the field inhomogeneity within the image voxel (Bernstein *et al.* 2004):

$$\frac{1}{T_2^*} = \frac{1}{T_2} + \frac{1}{T_2'}$$

(5.11)

Whereas T_2' is common for both the fat and water signals, T_2 differs between the two. In addition, there are also differences in T_2 values of the individual fat resonances.

A number of strategies have been suggested to consider T_2^* relaxation, and the optimal choice is dependent on application. Mainly, the strategies can be categorized into the following: 1) Estimation of a common T_2', 2) *a priori* knowledge of the individual T_2 values in combination with estimation of a common T_2', and 3) independent estimation of separate T_2^* values. Out of these, the second is of special interest in this thesis as it was suggested in **Paper I** for quantification of low fat contents, and has subsequently also been used and investigated for the purpose of quantification of fatty acid composition in **Papers IV and V**.

5.3.1 Estimation of a common T_2'

In fat/water separation and quantification, the differences in T_2 are often ignored and only the T_2' dephasing is modeled according to:

$$S(x, y, t_n) = [\rho_w(x, y) + \rho_f(x, y)e^{i2\pi\Delta f t_n}]e^{i2\pi\widehat{\psi}(x,y)t_n} \qquad (5.12)$$

where a complex field map is defined as:

$$\widehat{\psi} = \psi + \frac{i}{2\pi T_2{}'} \qquad (5.13)$$

Using this notation, both the off-resonance frequency and $T_2{}'$ may be estimated as a single complex parameter where ψ and $T_2{}'$ are obtained from the real and imaginary parts, respectively. Thus, inclusion of a common $T_2{}'$ does not increase the complexity of the iterative algorithm and the matrix notation is identical to that of simple off-resonance frequency estimation if ψ is replaced with $\widehat{\psi}$ in the matrices $\mathbf{B}$ and $\mathbf{D}$. (Yu, McKenzie, *et al.* 2007)

Estimation of a single, joint $T_2{}'$ is superior from an accuracy point of view to not including any $T_2{}^*$ dephasing in the signal model (Bydder *et al.* 2008, Hines *et al.* 2009, Hernando, Liang, *et al.* 2010, Hines *et al.* 2010, Meisamy *et al.* 2011, Reeder *et al.* 2012), and it becomes especially important when investigated after SPIO administration which lowers the liver $T_2{}^*$ (Bydder *et al.* 2010, Hines *et al.* 2012) or in the presence of hepatic iron deposition (Kang *et al.* 2012). However, the inclusion of $T_2{}'$ in the signal model does reduce the NSA (Hernando, Liang, *et al.* 2010, Reeder *et al.* 2012).
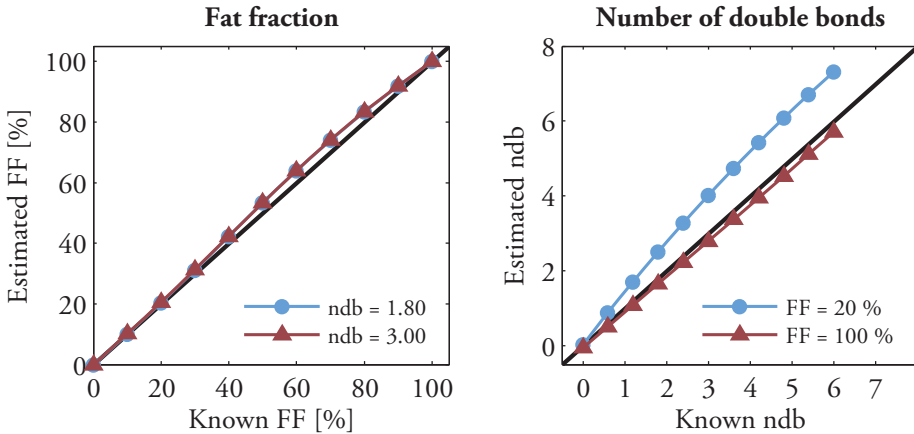

Figure 9. Bias of the estimated fat fraction and number of double bonds when correcting for a joint $T_2{}'$ dephasing only. Whereas very small bias is seen for the estimated fat fraction and for the number of double bonds in pure fat, the number of double bonds in fat/water mixtures are clearly overestimated. (Paper V)

This is the most common approach of T_2^* correction and was used in **Papers II and III**. However, there are cases in which inclusion of a single T_2' is not enough. In **Paper I**, it was demonstrated that this model is not sufficiently accurate when the sampling time is long or for applications where the expected difference in water and fat T_2^* is large. In addition, the results from **Paper V** indicate biased results of the fatty acid composition parameters in fat/water mixtures (see Figure 9). In these cases, it may be necessary to also include differences in T_2 of the various signal species.

5.3.2 Estimation of individual T_2^* of fat and water

Methods have also been suggested to estimate individual T_2^* of the fat and water signals (Bydder *et al.* 2008, Chebrolu *et al.* 2010). However, in this case the complexity of the estimation increases as five unknowns now need to be estimated: ψ, ρ_w, ρ_f, and the T_2^* of fat and water, respectively, and the same iterative linear least squares approach is not possible for separation (Chebrolu *et al.* 2010).

The potential improvement in accuracy from estimating independent T_2^* values of the fat and water signals has been investigated, mostly for liver applications, and has been found to be small in comparison to the degradation of the noise performance compared to modeling of a single T_2' (Bydder *et al.* 2010, Hernando, Liang*, et al.* 2010, Reeder *et al.* 2012, Horng *et al.* 2013). This is especially true in very low or very high FFs (Hernando, Liang*, et al.* 2010), such as in muscle applications. In these ranges, an alternative which does not impair estimation precision may thus be needed.

5.3.3 Combination of *a priori* knowledge and iterative estimation

In **Paper I**, an extension of the single T_2' model was suggested which uses *a priori* knowledge of the individual fat and water T_2 values:

$$
\begin{aligned}
S(x, y, t_n) = [\rho_w(x,y)e^{-\frac{t_n}{T_{2w}}} \\
+ \rho_f(x,y)e^{-\frac{t_n}{T_{2f}}}e^{i2\pi\Delta f t_n}]e^{i2\pi\hat{\psi}(x,y)t_n}
\end{aligned}
\tag{5.14}
$$

In this expression, the individual T_2 values of water and fat are denoted by T_{2w} and T_{2f}, respectively. Using this approach, the matrix **A** is adjusted according to:

$$\mathbf{A}_{Nx2} = \begin{bmatrix} e^{-\frac{t_1}{T_{2w}}} & e^{-\frac{t_1}{T_{2f}}} e^{i2\pi\Delta f t_1} \\ e^{-\frac{t_2}{T_{2w}}} & e^{-\frac{t_2}{T_{2f}}} e^{i2\pi\Delta f t_2} \\ \vdots & \vdots \\ e^{-\frac{t_N}{T_{2w}}} & e^{-\frac{t_N}{T_{2f}}} e^{i2\pi\Delta f t_N} \end{bmatrix} \tag{5.15}$$

The main advantage of this approach is that it does not require estimation of any additional parameters. However, it does require *a priori* knowledge of the fat and water T_2 values, which may be obtained from literature values, or complementary spectroscopy measurements. For liver applications, the range of fat and water T_2 values is approximately 40 ms – 65 ms and 15 ms – 40 ms, respectively (Hamilton *et al.* 2013). Alternatively, the difference between the fat and water T_2 values may be assumed known *a priori* as was done by Bydder *et al.* (Bydder *et al.* 2008).

In **Paper I**, this approach was found to increase accuracy while not degrading precision in case of a long sampling time and a large difference between the fat and water T_2 values compared to modeling a single T_2'. In addition, a large improvement of accuracy of estimated fatty acid composition parameters was demonstrated using this approach in **Paper V**. However, it was also seen that the success of the approach may be dependent on the choice of accurate T_2 values, especially for the water signal (see Figure 10).
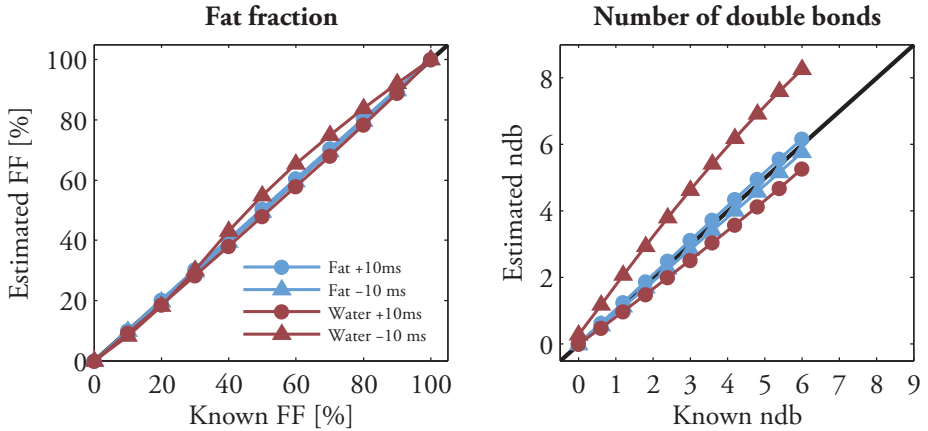

Figure 10. Bias of the estimated fat fraction and number of double bonds given that the actual fat and water T_2 values are ±10 ms relative to the modeled values. Whereas the bias associated with errors in the fat T_2 value is small, an overestimation of the water T_2 have a large impact on quantification accuracy. (Paper V)

5.4 Multi-peak fat spectrum

So far, a single fat resonance has been assumed and set to that of methylene at approximately -3.4 ppm relative to water. However, as discussed in Section 3.3.1, this is not a valid assumption. Instead, each of M fat resonances may be modeled according to the following equation assuming a single T_2' relaxation (Yu *et al.* 2008):

$$S(x,y,t_n) = [\rho_w(x,y) + \rho_f(x,y) \sum_{m=1}^{M} \alpha_m e^{i2\pi\Delta f_m t_n}]e^{i2\pi\hat{\psi}(x,y)t_n} \quad (5.16)$$

The relative contribution of the mth fat resonance is denoted by α_m [au] and the frequency shift relative to water by Δf_m [Hz]. These variables are assumed known *a priori* and therefore the complexity of the decomposition algorithm is not affected. The model requires only an update of the matrix **A**:

$$\mathbf{A}_{Nx2} = \begin{bmatrix} 1 & \sum_{m=1}^{M} \alpha_m e^{i2\pi\Delta f_m t_1} \\ 1 & \sum_{m=1}^{M} \alpha_m e^{i2\pi\Delta f_m t_2} \\ \vdots & \vdots \\ 1 & \sum_{m=1}^{M} \alpha_m e^{i2\pi\Delta f_m t_N} \end{bmatrix} \quad (5.17)$$

The frequency spectrum is well known for ectopic fat, but may shift relative to water due to temperature differences in e.g. phantoms, or due to bulk susceptibility effects of e.g. intermuscular fat (see Section 3.3.1). As demonstrated in **Paper I** and in the work by Karampinos *et al.* (Karampinos, Yu, *et al.* 2012), the impact on accuracy from this uncertainty may be decreased using a shorter sampling scheme (see Figure 11). The relative amplitudes for a specific organ may be obtained from literature, or they may be estimated knowing the approximate fatty acid composition (Hamilton, Yokoo, *et al.* 2011). Alternatively, complementary MRS measurements may be conducted, or imaging-based auto-calibration techniques have been suggested (Yu *et al.* 2008).

The superior accuracy of using a multi-peak fat spectrum compared to a single-peak model has been demonstrated in several investigations (Hines *et al.* 2009, Reeder *et al.* 2009, Hernando, Liang, *et al.* 2010, Hines *et al.* 2010, Meisamy *et al.* 2011). Thus, consideration of the multi-peak fat spectrum was included in all papers of this thesis.
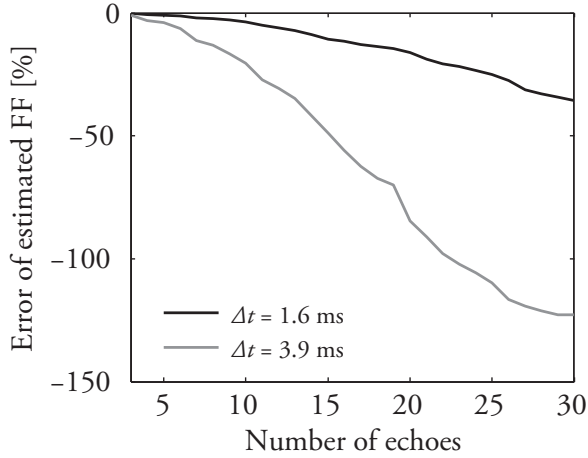
Figure 11. Percentage error of the estimated fat fraction (FF = 20 %) using a 0.05 ppm shifted fat model (e.g. due to bulk susceptibility effects or temperature differences) as function of the number of echoes with t_1 = 1.4 ms and inter-echo times 1.6 ms (black) and 3.9 ms (gray) at 3 T. It is evident that a shorter sampling reduces the effect of an inaccurate fat model.

5.4.1 Simultaneous estimation of fat content and fatty acid composition

Due to the generalized nature of the signal model and estimation process described in this chapter, it is easy to adapt the model to estimation of several signal species. Potentially, this opens up for the possibility to estimate water and each of the individual fat resonances, or specific clusters of resonances (see **preliminary report ii**) (Yu *et al.* 2008). Alternatively, theoretical knowledge of the chemical composition of fat may be used to simplify the model and reduce the number of unknowns. Such a model was suggested for an MRS application in 2011 (Hamilton, Yokoo*, et al.* 2011). The authors noted that the number of hydrogen atoms (and thus the proton-density-weighted signal intensity) in certain positions of the fatty acid chain was dependent on three factors: the number of double bonds *ndb* in the triglyceride molecule (-CH=CH-), the number of methylene-interrupted double bonds *nmidb* per triglyceride molecule (-CH=CH-CH$_2$-CH=CH-), and the average chain length *cl* of the fatty acids (number of carbon atoms). The expected amplitudes of the various fat signal components could therefore be expressed in terms of these parameters as summarized in Table 4. E.g., as the two hydrogen atoms contributing to peak 3 are present in each methylene-interrupted double bond group (-CH=CH-CH$_2$-CH=CH-), the theoretical amplitude of peak 3 is *2nmidb*.

Table 4. Assignment and generalized theoretical amplitudes expressed in terms of *ndb*, *nmidb*, and *cl* of eight individual fat resonances. The hydrogen atoms of interest are written in bold text.

Peak number	Chemical shift (ppm)[a]	Assignment	Theoretical amplitude
1	5.29	-C**H**=C**H**-	$2ndb+1$
	5.19	-C**H**-O-CO-	
2	4.20	-C**H₂**-O-CO	4
3	2.75	-CH=CH-C**H₂**-CH=CH-	$2nmidb$
4	2.24	-CH₂-C**H₂**-COO	6
5	2.02	-C**H₂**-CH=CH-	$4(ndb\text{-}nmidb)$
6	1.60	-C**H₂**-CH₂-COO	6
7	1.30	-(C**H₂**)$_n$-	$6(cl\text{-}4)\text{-}8ndb+2nmidb$
8	0.90	-CH₂-C**H₃**	9

[a] As observed in the liver by Hamilton *et al.* (Hamilton, Yokoo*, et al.* 2011)

In **Paper IV**, an imaging-based approach of mapping each of these fatty acid composition parameters was introduced. Alternative approaches have also been presented by Berglund *et al.* (Berglund *et al.* 2012) and Bydder *et al.* (Bydder *et al.* 2011). Whereas Bydder *et al.* use empirical relations between the three parameters to further simplify the problem, Berglund *et al.* and **Paper IV** independently map all three parameters.

The derivation of the algorithm proposed and evaluated in **Paper IV** is based on eq. 5.16, but with the addition of individual T_2 values of each individual fat resonance. In this signal expression, each of the relative amplitudes of the individual fat resonances was replaced by the theoretical amplitudes given in Table 4. However, as the theoretical amplitudes are not normalized, a normalization factor k is defined as the sum of the theoretical amplitudes of all fat peaks:

$$k = \frac{1}{\sum_{m=1}^{M} \alpha_m} = \frac{1}{6cl - 2ndb + 2} \tag{5.18}$$

From the resulting expression, it is possible to group the included fat signal contributions according to those weighted by $\rho_f k$, $\rho_f k \cdot ndb$, $\rho_f k \cdot nmidb$, and $\rho_f k \cdot cl$. Thus, each of the fatty acid composition parameters may be modeled as a cluster of differently weighted fat resonances according to the following adapted matrices $\boldsymbol{\rho_{5x1}}$ and $\mathbf{A}_{Nx5}$:

$$\rho = \begin{bmatrix} \rho_w(x,y) \\ \rho_f k(x,y) \\ \rho_f k \cdot ndb(x,y) \\ \rho_f k \cdot nmidb(x,y) \\ \rho_f k \cdot cl(x,y) \end{bmatrix} \tag{5.19}$$

$$A = \begin{bmatrix} e^{-\frac{t_1}{T_{2w}}} & a(t_1) & b(t_1) & c(t_1) & d(t_1) \\ e^{-\frac{t_2}{T_{2w}}} & a(t_2) & b(t_2) & c(t_2) & d(t_2) \\ \vdots & \vdots & \vdots & \vdots & \vdots \\ e^{-\frac{t_N}{T_{2w}}} & a(t_3) & b(t_N) & c(t_N) & d(t_N) \end{bmatrix} \tag{5.20}$$

with:

$$
\begin{aligned}
a(t_n) &= E_1(t_n) + 4E_2(t_n) + 6E_4(t_n) + 6E_6(t_n) - 24E_7(t_n) \\
&\quad + 9E_8(t_n) \\
b(t_n) &= 2E_1(t_n) + 4E_5(t_n) - 8E_7(t_n) \\
c(t_n) &= 2E_3(t_n) - 4E_5(t_n) + 2E_7(t_n) \\
d(t_n) &= 6E_7(t_n)
\end{aligned}
\tag{5.21}
$$

In these expressions, $E_m = e^{i2\pi\Delta f_m t_n} e^{-t_n/T_{2m}}$ was defined for simplicity. From $\boldsymbol{\rho}$, it is easy to estimate the parameters ρ_w, ρ_f, *ndb*, *nmidb*, and *cl*.

The use of the multi-peak fat spectrum for quantification of the fatty acid composition is a new field and thus, the evaluation of method performance is so far limited to a few studies. In **Paper IV**, the accuracy of the technique was investigated in a wide range of both fat contents and fatty acid compositions (see Figure 12), and compared to that of an MRS technique. In pure oil, a promising agreement with known values was found, but the accuracy in fat/water mixtures was slightly lower. Encouragingly, the detected accuracy of the technique was found to be similar to that of MRS. Similar promising accuracies were found in pure oil in the works by Bydder *et al.* and Berglund *et al.* (Bydder *et al.* 2011, Berglund *et al.* 2012). In addition, a high reproducibility has been reported for the estimation of all fatty acid composition parameters but *cl*, which appeared less robust (Berglund *et al.* 2012).
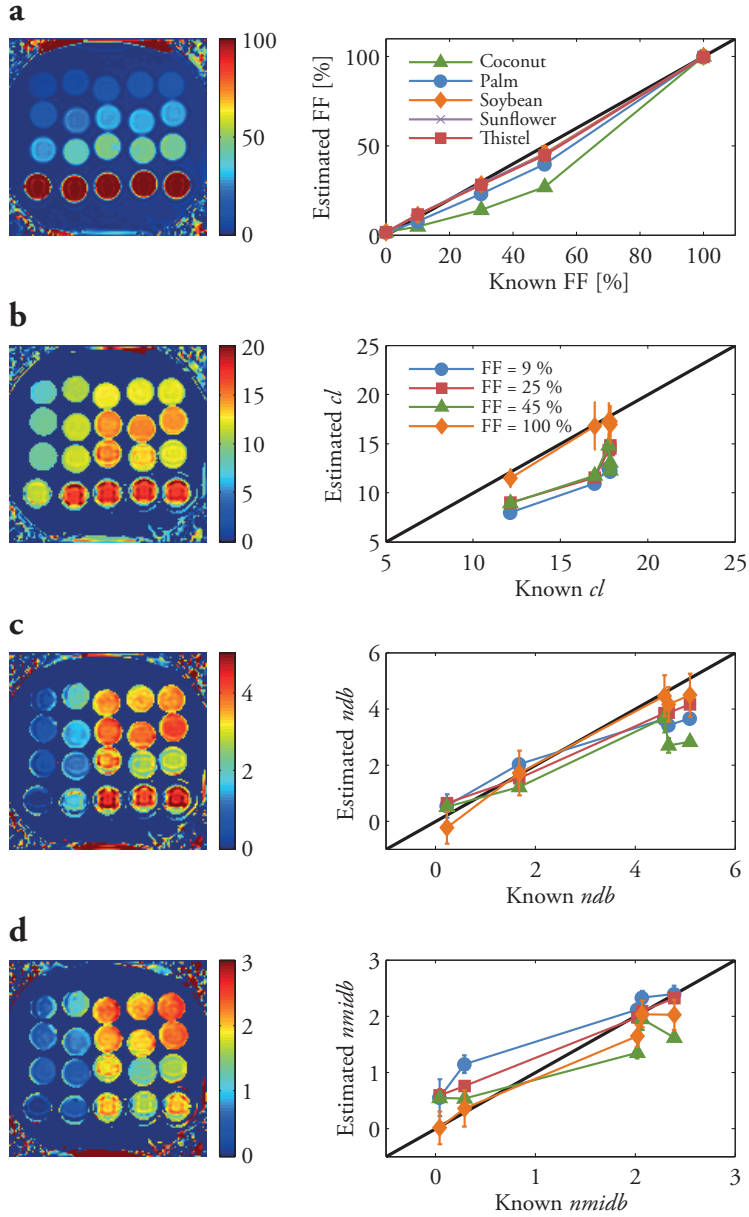
Figure 12. Example maps and scatter plots compared to known values of estimated FF (a), *cl* (b), *ndb* (c), and *nmidb* (d) of emulsion gel phantoms of various compositions and FFs. Each phantom column represents a fatty acid composition, and each row represents a FF. A promising accuracy is seen in pure oil (orange diamonds), but slightly lower accuracy is seen in fat/water mixtures. (Paper IV)

5.5 Errors due to a bipolar acquisition scheme

A more efficient image acquisition may be performed using bipolar instead of unipolar read-out gradients. In **Paper III**, the accuracy and noise performance of this technique were investigated for fat quantification purposes.

A number of artifacts make fat/water separation and quantification more difficult when using a bipolar acquisition scheme. Chemical-shift displacement and distortions due to an inhomogeneous field both occur in opposite direction in every other echo. The chemical-shift distortion may be corrected by performing the fat/water separation in k-space, or be neglected in case of a high bandwidth (Lu *et al.* 2008). Field-inhomogeneity distortions may be corrected using the estimated field map, or be ignored in case of typical shimming conditions (Lu *et al.* 2008).
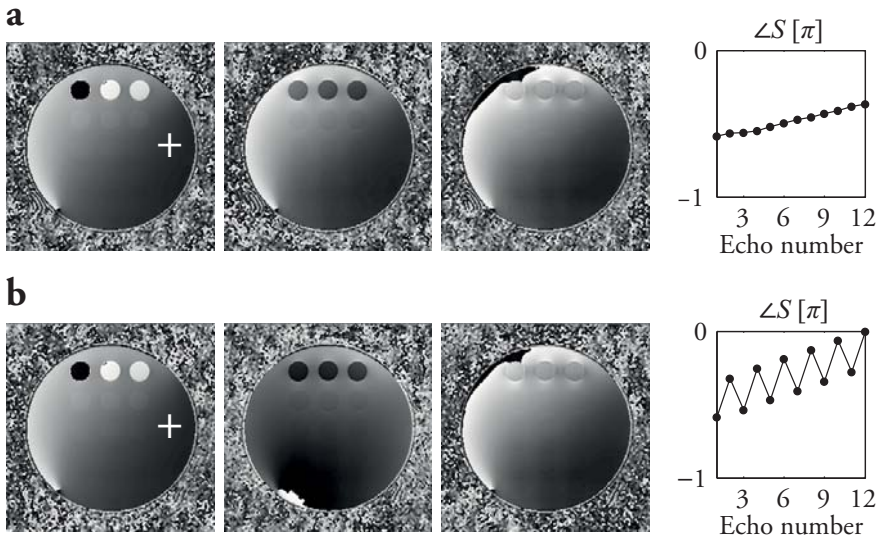

Figure 13. Phase images from a phantom experiment using identical echo times with a unipolar (a) and bipolar (b) read-out mode. The images show the first to third echoes, and the phase ($\angle S$) at the voxel denoted + is plotted against echo number for each of the twelve echoes. Whereas a smooth phase evolution with echo time is seen for the unipolar read out, clear phase discrepancies with every other echo are evident for the bipolar read out.

More detrimental to the field of fat/water separation are the phase and amplitude errors. First, phase errors occur when the k-space line acquired is not perfectly centered in k-space due to gradient delays or eddy currents. Such a shift in k-space results in a linear phase error of the image after the Fourier transform (see Figure 13). Although the phase errors are mainly linear, they may also include higher order terms (Eggers *et al.* 2008, Yu *et al.* 2010). Especially, phase errors are expected to be large off-center in the read-out direction of the image. Second, the frequency-dependence of the receiver-coil

40

sensitivity cause an amplitude variation over the read-out direction, again being of opposite direction in every other echo (Eggers *et al.* 2008, Yu *et al.* 2010).

Several papers have addressed these errors. Some of them focus on the phase errors and suggest a correction of the linear phase errors only (Leupold *et al.* 2006, Lu *et al.* 2008). Others require reference scans or a modified pulse sequence to address amplitude- and phase errors in more detail (Li *et al.* 2007, Yu *et al.* 2010). Also, a built-in correction of the phase errors only have been suggested (Eggers *et al.* 2011).

In **Paper III**, an algorithm was investigated which uses modeling of the effects to correct both type of errors in all spatial directions jointly with the fat/water separation. Let us denote the phase errors ϕ [rad] and the amplitude demodulation ε [au] and define a complex error map θ according to:

$$\theta(x,y) = \phi(x,y) - i\varepsilon(x,y) \tag{5.22}$$

Using this formulation, the signal equation (based on eq. 5.12) may be altered according to the following to account for a bipolar acquisition scheme. A single fat frequency was assumed for simplicity of the description, however, a multi-peak model is easily implemented.

$$S(x,y,t_n) = \big[\rho_w(x,y) + \rho_f(x,y)e^{i2\pi\Delta f t_n}\big]e^{i2\pi\widehat{\psi}(x,y)t_n}e^{(-1)^n i\theta(x,y)} \tag{5.23}$$

In this expression, the term $e^{(-1)^n i\theta}$ represents a modulation of the signal with frequency $1/\Delta t$ (see Figure 13). The extension yields an additional error matrix $\mathbf{\Theta}_{NxN}$ in the matrix notation of the signal expression:

$$\mathbf{S} = \mathbf{\Theta D A \rho} \tag{5.24}$$

As before, the matrices $\mathbf{D}$, $\mathbf{A}$, and $\mathbf{\rho}$ are adaptable to the signal model chosen and the matrix $\mathbf{\Theta}$ is defined according to:
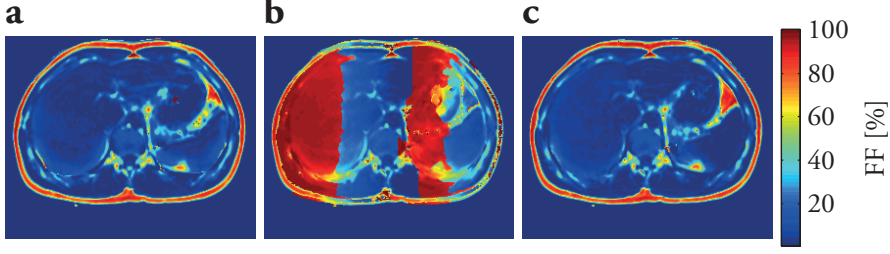
Figure 14. An axial slice acquired through the liver of a healthy volunteer using unipolar (a) and bipolar gradients (b-c). The artifacts are evident in b), where no correction is made, but no artifacts are present when the bipolar correction algorithm is used (c). (Paper III)

$$
\mathbf{\Theta}_{NxN} = \begin{bmatrix} e^{(-1)^1 i\theta(x,y)} & 0 & \cdots & 0 \\ 0 & e^{(-1)^2 i\theta(x,y)} & \cdots & 0 \\ \vdots & \vdots & \ddots & \vdots \\ 0 & 0 & \cdots & e^{(-1)^N i\theta(x,y)} \end{bmatrix} \tag{5.25}
$$

Similar to the estimation of the complex field map, the complex error map may be linearized by a Taylor expansion, and the matrix $\mathbf{B}_{NxP+2}$ is adjusted according to:

$$
\begin{aligned}
&\mathbf{B}_{NxP+2} \\
&= \begin{bmatrix} & (\tilde{\rho}_w + \tilde{\rho}_f e^{i2\pi\Delta f t_1})i2\pi t_1 & (\tilde{\rho}_w + \tilde{\rho}_f e^{i2\pi\Delta f t_1})(-1)^1 i \\ \mathbf{A} & (\tilde{\rho}_w + \tilde{\rho}_f e^{i2\pi\Delta f t_2})i2\pi t_2 & (\tilde{\rho}_w + \tilde{\rho}_f e^{i2\pi\Delta f t_1})(-1)^2 i \\ & \vdots & \vdots \\ & (\tilde{\rho}_w + \tilde{\rho}_f e^{i2\pi\Delta f t_N})i2\pi t_N & (\tilde{\rho}_w + \tilde{\rho}_f e^{i2\pi\Delta f t_1})(-1)^N i \end{bmatrix}
\end{aligned} \tag{5.26}
$$

With this formulation, both the complex error map and the complex field map may be estimated using the iterative procedure described in Chapter 5.2, and the following expression:

$$
\begin{bmatrix} \Delta\tilde{\rho}_w(x,y) \\ \Delta\tilde{\rho}_f(x,y) \\ \Delta\tilde{\tilde{\psi}}(x,y) \\ \Delta\tilde{\theta}(x,y) \end{bmatrix} = (\mathbf{B}^T\mathbf{B})^{-1}\mathbf{B}^T(\mathbf{D}^{-1}\mathbf{\Theta}^{-1}\mathbf{S} - \mathbf{A}\tilde{\boldsymbol{\rho}}) \tag{5.27}
$$

Similar methods have also been described in preliminary reports (see **preliminary report v**) (Eggers *et al.* 2008).

Much like for the estimation of the complex field map, an initial guess may be necessary to guide the iterative estimation of the complex error map in case of large errors. In **Paper III**, the linear phase errors were estimated from the first three echoes by the approximate expression:

$$\phi(x,y) \approx \frac{1}{4} \angle \left(\frac{S(t_2,x,y)^2}{S(t_1,x,y) \cdot S(t_3,x,y)} \right) \tag{5.28}$$

As the expression is susceptible to phase wraps, a first-degree polynomial is fitted to the center columns of the ϕ map where errors are expected to be small.
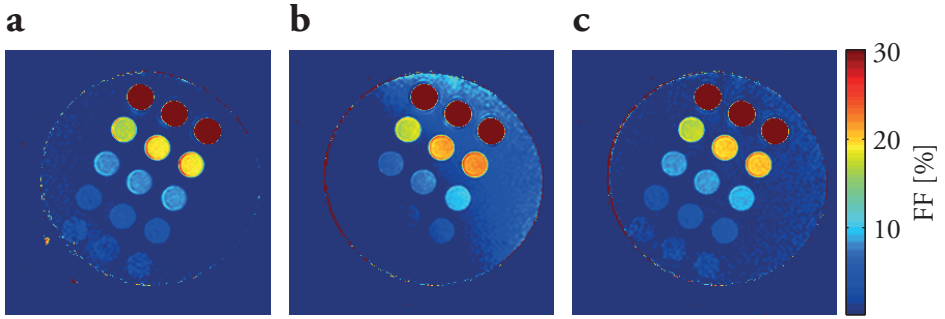

Figure 15. FF images of a phantom consisting of pure oil (top row) and various Intralipid dilutions (FF = 20 %, 10 %, 5 %, and 2.5 % from top to bottom) using a unipolar (a), and bipolar acquisition (b,c). Residual artifacts are seen when using a low order correction (b), but are improved using a full correction of both phase and amplitude errors (c). The color scale was set to range between 0 % and 30 % for better visualization of the artifacts. (Paper III)

Several studies focus on the use of a bipolar acquisition scheme for fat/water separation purposes only (Leupold *et al.* 2006, Li *et al.* 2007, Eggers *et al.* 2008, Lu *et al.* 2008, Yu *et al.* 2010, Eggers *et al.* 2011). However, to the best of the author's knowledge, **Paper III** is the only study which investigates the accuracy and noise performance of using this technique for fat quantification. The approach was demonstrated to effectively correct for the associated artifacts in the liver of a healthy volunteer (see Figure 14). Also, it was found that using a built-in correction via signal modeling, the quantification accuracy and noise performance of a bipolar acquisition scheme was similar to the unipolar case (see Figure 7). In addition, the quantification accuracy was superior to a low-order correction of the linear phase errors only (see Figure 15). However, the choice of echo spacing was found more limited compared to the unipolar case, as an additional dip in NSA was present for a π inter-echo shift (see Figure 7).

43

5.6 Summary

In the almost 30 years that have passed since the first introduction of Water/Fat Imaging, the initial 2-point technique has been extended and generalized to allow for a flexible sampling scheme with inclusion of a detailed signal model. For accurate separation of the fat and water signals, or various fat signals, it is necessary to include the estimation of an off-resonance frequency and joint T_2' dephasing. It is also vital to include accurate modeling of the multi-peak fat spectrum, which may be included without adding complexity to the algorithm.

From the results of this thesis, the use of a complex reconstruction may be recommended (**Paper I**). In addition, the use of *a priori* T_2 values of fat and water increase accuracy of the estimation of fat content and fatty acid composition without degrading the noise performance (**Papers I, IV, and V**). Using a built-in correction of the associated artifacts, accurate fat quantification is possible using a bipolar acquisition scheme (**Paper III**). Finally, an imaging-based algorithm for estimation of the fatty acid composition has been suggested and show promising accuracy (**Paper IV**).

6. Quantification

One of the most fascinating properties of MR imaging is the many sources of image contrast and the many ways in which their respective influences may be manipulated. For quantitative purposes, one source of image contrast needs to be isolated. Thus, to obtain a truly quantitative fat measure using the sorted fat and water images, several potential sources of bias need to be considered in addition to the effects discussed for the fat/water separation step. In this chapter, various methods to address potential sources of bias in quantification of fat content and fatty acid composition are described and their performance reviewed. Especially the impact on quantification accuracy from T_1 weighting and the potential advantages of using a fat reference for quantification has been investigated in this thesis.

6.1 Definition of a quantitative measure

The separated fat and water signal components are just that: signals. Their intensities are dependent on a number of factors, in addition to the fat and water contents such as the imaging parameters and the B_1 field. To obtain a quantitative measure which is indicative of the fat content only, each of these factors need to be addressed. A fat proton density percentage may be calculated by relating the fat signal in each image voxel to a reference signal: either water or pure fat. Of these, the use of a water reference is the simplest and by far the most commonly used.

6.1.1 Water reference

The percentage fat protons within a voxel, or the proton density fat fraction FF, may be obtained by relating the fat signal to the total signal. Assuming that the signal consist of the unweighted fat ρ_{f0} and water ρ_{w0} signals only, the proton density FF is defined as (Buxton *et al.* 1986):

$$FF(x,y) = \frac{\rho_{f0}(x,y)}{\rho_{f0}(x,y) + \rho_{w0}(x,y)} \tag{6.1}$$

As both the fat and water signals are expected to be equally affected by coil sensitivity and transmit RF inhomogeneity, these effects are cancelled in the FF parameter. However, the Rician noise distribution of magnitude data at low SNRs cause an overestimation of the FF in case of low fat contents if the magnitude of the water and fat signals are used for FF estimation (Gudbjartsson and Patz 1995, Liu *et al.* 2007). Instead, the phase of the estimated parameters may be assumed equal at a zero echo time and the real-valued FF used to avoid noise bias.

A very strong correlation has been demonstrated between the proton density FF and the triglyceride mass fraction as measured using chemical analysis of extracted samples (Hu *et al.* 2011, Artz *et al.* 2012, Hines *et al.* 2012). Thus, the proton density FF is a strong indicator of tissue fat content.

6.1.2 Fat reference

Instead of relating the fat signal to the total signal, it is possible to relate the fat signal to the signal in pure fat. The resulting measure will be referred to as the fat reference fat fraction fFF. The measure may not be dependent on the use of unweighted signals assuming that fat is equally weighted over the entire image. Thus, the SNR may be increased using a higher flip angle without compromising quantification accuracy (see further below). However, a pure fat reference need to somehow be defined. In addition, the coil sensitivity and RF homogeneity are not cancelled as the fat reference is taken from a separate region of the image.

In **Paper II**, the Multi Scale Adaptive Normalized Averaging (MANA) algorithm is used for correction of B_1 inhomogeneitites and fat reference selection (Leinhard *et al.* 2008, Romu *et al.* 2011). In this case, B_1 inhomogeneities are corrected using an intensity interpolation assuming that all adipose tissue should have equal signal intensity in case of a homogenous B_1 field. Adipose tissue within the image is used as a fat reference and is automatically selected using a threshold FF value. Other approaches have included no correction of B_1 inhomogeneities (Hu and Nayak 2008) or separate B_1-mapping scans (Cui *et al.* 2012). Also, the use of an external fat reference have been suggested (e.g. an oil phantom) (Cui *et al.* 2012).

To the best of the author's knowledge, **Paper II** is the only study comparing the quantification accuracies of fat and water reference approaches (see example FF and fFF maps in Figure 16). In this paper, the accuracy, precision, and repeatability of using a fat reference for FF estimation were all similar to that of a water reference FF in case of identical imaging parameters. However, consideration of image resolution was more important for the estimation of fFF as it needed to be sufficient to resolve the adipose tissue for use as an internal fat reference.
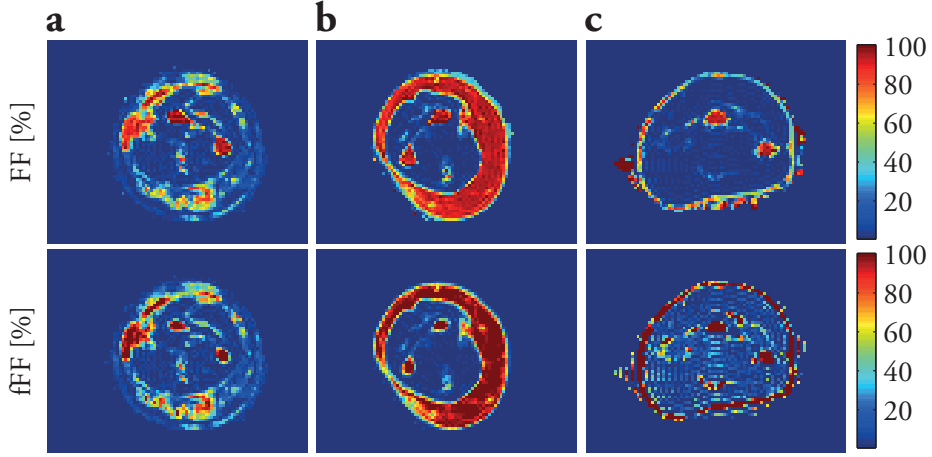
Figure 16. Example FF (upper row) and fFF maps (lower row) from the edematous, liposuctioned arm (a) and healthy arm (b) of a patient subject as well as from the right arm of a healthy volunteer (c). Whereas successful reconstructions of the fFF are seen in a) and b), the reference fat tissue was not sufficient for fFF reconstruction in c). (Paper II)

6.2 Weighting of image contrast

The intensity of the separated fat and water signals with T_1 values T_{1f} and T_{1w}, respectively, depend on the choice of image parameters according to the signal expression of a gradient echo sequence (Bernstein *et al.* 2004):

$$\rho_{w,f}(a, TR, x, y) = \rho_{w0,f0}(x, y) \frac{\sin(a)\left(1 - e^{-\frac{TR}{T_{1w,f}}}\right)}{1 - \cos(a)\, e^{-\frac{TR}{T_{1w,f}}}} \tag{6.2}$$

In this expression, the water and fat signals at an infinite TR and a zero echo time are denoted ρ_{w0} and ρ_{f0}, respectively, and the flip angle is denoted a. Of course, also the T_2^* relaxation affects the signal, but is already included in the signal-evolution equations given in the fat/water separation description.

Using a water reference, the difference in T_{1w} and T_{1f} causes an overestimation of the estimated FF as the fat and water signals are differently weighted (see Figure 17-Figure 18) (Liu *et al.* 2007, Bydder *et al.* 2008). This effect is well known and was verified also in **Paper II**. On the contrary, **Paper V** is the first to investigate the potential T_1 bias of

the quantification of fatty acid composition. In this study, T_1 weighting was shown to have rather small impact on the quantification of fatty acid composition parameters (see Figure 17). Thus, some T_1 weighting may be allowed in order to increase SNR for quantification of the fatty acid composition.

However, the effect on the quantification of FF is evident and cannot be neglected. To account for this issue, several approaches have been suggested: 1) A small flip angle approach, 2) correction using *a priori* T_1 values, 3) simultaneous T_1 mapping, and 4) the use of a fat reference for quantification. Each of these approaches are further discussed below. Of these, the use of a fat reference was of special interest in this thesis (**Paper II**).
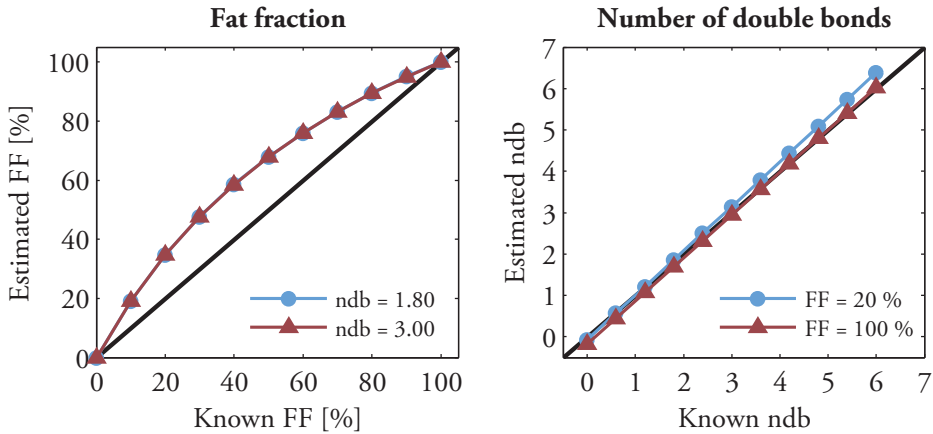

Figure 17. Impact of T_1 weighting on the quantification accuracy of the FF and the *ndb* for various FFs and fatty acid compositions. FF estimation is more affected by T_1-related bias than estimation of the fatty acid composition. (Paper V)

6.2.1.1 Small flip angle

T_1-related bias may be avoided by choosing the *a*/TR pair such that T_1 weighing is negligible (Bydder *et al.* 2008). The optimal *a*/TR pair of course depends on the level of T_1 bias which is considered negligible for the current application and the T_1 values of fat and water. Although the use of a small flip angle is attractively simple, and often used for e.g. liver applications (Reeder *et al.* 2011), this approach limits the SNR achievable in a reasonable imaging time. Especially the quantification of low FFs may be improved if T_1 weighting is used to enhance the low fat signal (**Paper II**). Thus, the use of a higher flip angle may be advantageous, but calls for correction of the associated T_1 bias.
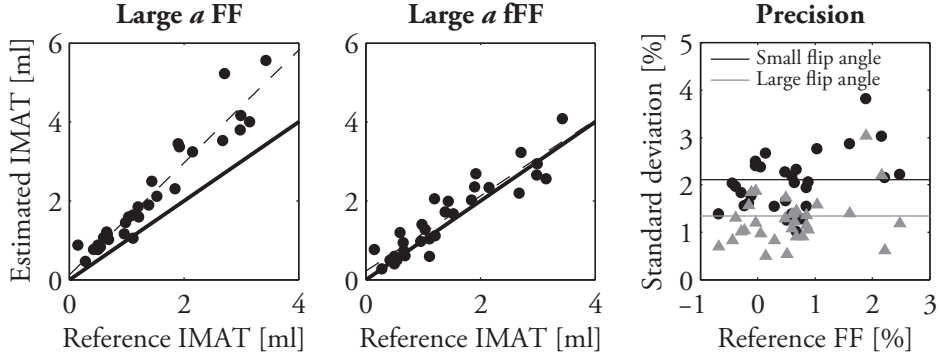
Figure 18. Scatter plots comparing the IMAT volumes estimated from a large flip angle FF (right) and large flip angle fFF (middle) to those from a small flip angle FF. The TR was set to 600 ms and the small/large flip angles to 10°/85°, respectively. The precision of the small flip FF and large flip angle fFF are compared to the left. The use of a large flip angle effectively avoids T_1 bias and improves precision compared to a small flip angle FF. (Paper II)

6.2.1.2 Correction using a priori T_1 values

Instead of a small flip angle, a larger flip angle may be chosen and *a priori* T_1 values may be used to correct for the bias by estimation of the $\rho_{w0,f0}$ from $\rho_{w,f}$. The accuracy of this approach is of course dependent on the choice of T_1 values, but even more so on accurate knowledge of the flip angle actually used (Yang *et al.* 2013). To account for these uncertainties, it may be necessary to map fat and water T_1 values, and possibly the B_1 field, on an individual basis.

6.2.1.3 Simultaneous T_1 mapping

To simultaneously map the FF and the fat and water T_1 values, the fat/water separation may be performed from data acquired at two or more flip angles, or at several TRs (Buxton *et al.* 1986, Liu *et al.* 2007, Karampinos *et al.* 2011). The choice of optimal a/TR pairs for the estimation of the various parameters depend on the T_1 values expected (Buxton *et al.* 1986, Liu *et al.* 2007). Using a dual flip angle approach, the sensitivity of the estimated FF on uncertainties in the flip angles are effectively cancelled given that the relative errors of the two flip angles are similar (Liu *et al.* 2007). However, the approach is less noise efficient than the acquisition of a single flip angle data set for liver applications (Wiens *et al.* 2009). For skeletal muscle applications, the acquisition of two small, but unequal, flip angles have proven more noise efficient than acquisition of a single flip angle with identical scan time (Karampinos *et al.* 2011).

6.2.1.4 Use of a fat reference

Given the assumption that all fat signals are identically weighted, the use of a fat reference instead of a water reference circumvents T_1 bias as only fat signals is used for quantification (**Paper II**) (Hu and Nayak 2008). In **Paper II**, it is demonstrated that

this approach in combination with a larger flip angle does increase the precision of FF estimation with similar accuracy compared to a small flip angle FF estimation (see Figure 18). However, no improvement of repeatability was detected.

6.2.2 Parameter-dependent relaxation times

There have been reports on a FF dependence on the fat and water relaxation values (**Preliminary report vi**) (Hu and Nayak 2010). In addition, the author's own investigations indicate that there may be an *ndb* dependence on the T_2 of water and individual fat resonances (unpublished data). If present, these effects would have impact on any method requiring *a priori* knowledge of relaxation values, and the assumption that all fatty tissue is equally weighted may not be valid. Likely, parameter-dependent values are also of importance when performing method performance evaluation studies where a large range of FFs and fatty acid composition are imaged simultaneously. Thus, the effect might explain the lower quantification accuracy of fatty acid composition parameters in fat/water mixtures found in **Paper IV**.

6.3 Absolute fat quantification

The proton density FF is strongly correlated to the mass and percentage of triglycerides as measured using chemical analysis (Hu *et al.* 2011, Artz *et al.* 2012, Hines *et al.* 2012). However, the measures are not identical as the FF includes MR-visible components only, and compares the proton densities of fat and water as opposed to masses or volumes. Thus, for estimation of absolute fat mass or volume, corrections are necessary to account for proton density differences between fat and water (**Paper I and Paper IV**), and to consider the presence of MR-invisible components of the voxel (Longo *et al.* 1995, Hu *et al.* 2011). However, even without these, rather small, corrections, accurate estimation of the fat mass has been achieved (Hu *et al.* 2011). Therefore, no corrections were made for estimation of the IMAT volume from the proton density FF in **Paper II**:

$$IMAT = voxel\ volume \cdot \sum_{v}^{V} FF_v \qquad (6.3)$$

Using the fFF instead of the FF, both the need for correction of proton density differences of fat and water and the presence of MR-invisible water components are

avoided. However, the proton density of fat does need to be converted to fat mass or volume.

6.4 Summary

For a quantitative measure of the fat content which may be compared to independent measures and which is physiologically relevant, the proton density FF may be used. For unbiased estimation, T_1-related bias and noise need to be considered in addition to the sources of bias modeled for fat/water separation. Given these corrections, the proton density FF need very small correction for an absolute measure of the mass or volume fat. From the results of this thesis, it may additionally be concluded that some T_1-weighting may be allowed to increase SNR when estimating the fatty acid composition parameters with only very small impact of accuracy (**Paper V**). T_1 weighting may also be used to improve precision of low fat content estimation if a fat reference is used to avoid T_1-related bias (**Paper II**).

7. Discussion and conclusions

MRI-based fat quantification techniques have earned plenty of attention in recent years, and the techniques have become well established and appreciated, especially for applications in the liver. In addition, they have been validated against independent quantitative techniques (Hu *et al.* 2011, Artz *et al.* 2012, Hines *et al.* 2012), shown to have excellent diagnostic performance (Hines *et al.* 2011, Kang *et al.* 2012), and to provide a precise and reproducible FF measure (Hines *et al.* 2011, Kang *et al.* 2011). In this thesis, a number of method developments were described which widens the horizons of what is possible to measure.

7.1 Quantification of low fat concentrations

Quantification of low fat concentrations is of importance in measurements of fat accumulation in especially the heart or skeletal muscles. The specific challenges of fat quantification for these applications are the low fat contents expected, the large difference in especially the T_1 values of fat and water, and susceptibility effects. All of these issues were addressed in **Papers I and II**.

First, the feasibility of measuring FFs < 1 % was demonstrated using a phantom experiment (see Figure 19) (**Paper I**). Encouragingly, the accuracy and precision were similar to or better than those found using MRS (**Paper I**). *In vivo*, the approximate standard deviation in homogenous muscle tissue was estimated to approximately 2 % using a small flip angle and a water reference for quantification (**Paper II**). To further improve precision, the flip angle may be increased given that T_1 bias is considered. In **Paper II**, this was accomplished using a fat reference for quantification. The use of a large flip angle and a fat reference resulted in similar accuracy as the small flip angle water reference approach and improved precision, but not repeatability (**Paper II**). However, in case of a fat reference, the imaging resolution need to be considered and preferably a 3D acquisition of a larger volume may be used for proper resolving and inclusion of adipose tissue which is needed as a pure fat reference (**Paper II**).

Yet another approach of increasing SNR is the acquisition of a larger number of echoes. This approach was used in **Paper I**. However, this calls for careful consideration of susceptibility effects and accurate modeling of T_2^* dephasing as the effect on quantification accuracy of both tend to increase with an increasing sampling time

(**Paper I**). As the fat/water frequency shift increases with field strength, this point is even more important at 3 T than at 1.5 T (**Paper I**). Based on these findings, the *in vivo* experiments of **Paper II** were all conducted at 1.5 T with the shortest possible inter-echo time to reduce the impact of susceptibility effects and differences in T_2 of fat and water.

Currently, the techniques developed are used for a clinical study aiming at investigating fat and water distributions of the limbs of patients with lymphedema, and how these distributions change up to one year after liposuction. Some preliminary results have already been presented at international conferences (**preliminary reports iv and ix**).

In the future, a fascinating method development would be an imaging-based technique for separation of IMCL and EMCL in skeletal muscle. Currently this distinction is only possible using MRS, which provides limited spatial information, may require lengthy acquisition times, and requires evaluation by an experienced operator.
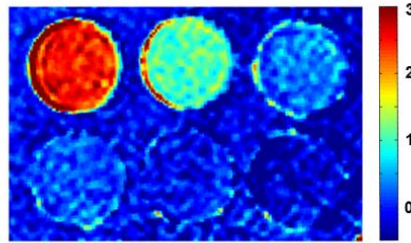

Figure 19. Example FF map of Intralipid phantom vials with FFs 0 % - 0.34 % (bottom right to left) and 0.68 % - 2.7 % (top right to left). The color scale is set to range from 0 % to 3 %. (Paper I)

7.2 Efficient data acquisition in fat quantification

The use of a bipolar acquisition scheme may be of importance for breath-hold applications and for applications which would gain from the use of multiple, tightly spaced echoes at especially higher field strengths. However, this approach require correction of the associated phase and amplitude errors which render reconstructed FF images useless. With insufficient correction, or due to the added estimation of these parameters, fat quantification accuracy and noise performance might suffer. Thus, in **Paper III**, the fat quantification accuracy and noise performance for a built-in correction of phase and amplitude errors were investigated for a bipolar acquisition scheme.

In **Paper III**, a low-order correction of linear phase errors only was proven insufficient for fat quantification purposes, but a complete built-in correction of both phase and

54

amplitude errors provided accurate FFs. An interesting result from this study was the very similar NSAs of the unipolar and bipolar separation algorithms in a wide range of inter-echo shifts. However, as the errors and the dominant fat signal are inseparable at a π inter-echo shift, the bipolar separation algorithm did result in an additional dip in NSA at this inter-echo shift.

Future research on the use of a bipolar acquisition scheme should include a validation study of fat quantification accuracy and precision *in vivo*, as only an *in vivo* feasibility demonstration was provided in **Paper III**. In addition, the potential gain in total scan time, inter-echo time, and number of obtainable echoes should be investigated compared to a unipolar acquisition scheme given the noise performances of the two methods.

7.3 Quantification of the fatty acid composition

The fatty acid composition is of interest in several applications, such as objective investigations of dietary habits, research on the various functions of different fatty depots, or possibly, for the distinction of simple hepatic steatosis and inflammatory conditions. Thanks to the flexible formulation of the Water/Fat Imaging problem and theoretical knowledge of the chemical structure of fatty acids, estimation of the fatty acid composition may be possible using Water/Fat Imaging. In **Paper IV**, a Water/Fat Imaging-based approach for quantification of the fatty acid composition was suggested, and its accuracy was compared to that of MRS *in vitro*. In **Paper V**, potential sources of bias of the estimated FF and fatty acid composition parameters were investigated.

The suggested technique showed promising accuracy, which was comparable or better than that of MRS in pure fat, whereas slightly lower accuracy was seen in fat/water mixtures using both techniques (**Paper IV**). In addition, a demonstration in the thigh adipose tissue of a healthy volunteer resulted in reasonable fatty acid composition parameters (see Figure 20) (**Paper IV**). However, especially the *cl* parameter appeared more sensitive to inaccuracies in the signal model (**Paper IV, Paper V**).

The noise performance of the technique was more sensitive to the choice of inter-echo shift compared to simple fat/water separation (**Paper IV**). Although only eight echoes were used for quantification in **Paper IV**, it is likely that the noise performance may be further improved if this number is increased (**Paper V**) (Berglund *et al.* 2012). However, it should also be noted that the accuracy of the technique is sensitive to an accurate fat frequency model, and this sensitivity may increase given a longer sampling time (**Paper IV, Paper I**).

A priori modeling of individual T_2 values of especially the water and dominant fat signal is vital for accurate quantification of fatty acid composition parameters in fat/water mixtures (**Paper V**). The accuracy of the modeled water T_2 value may be crucial, but is

less critical for the fat T_2 value (**Paper V**). However, contrary to what might be expected from FF quantification, the effect on fatty acid composition estimation from an inaccurate T_2 model did not increase with a longer sampling time (**Paper V**). Whereas very important for FF quantification, T_1-related bias appeared less influential on the accuracy of fatty acid composition parameters (**Paper V**). This may imply that at least some T_1 weighting may be used with sufficient accuracy to improve SNR in fat/water mixtures (**Paper V**).

Quantification of the fatty acid composition is a fascinating field in its very beginning and much research and method development is still needed. Approaches to decrease the sensitivity of the method to model inaccuracies should be investigated and further *in vivo* investigations, first of all in adipose tissue, are needed for validation of the technique. Even further in the future, the use of the technique for liver applications could potentially be very useful, but to meet that end, potential sources of bias need to be fully investigated and considered, the acquisition time needs to be compatible with a breath-hold, and the accuracy of the resulting measures need to be validated *in vivo*.
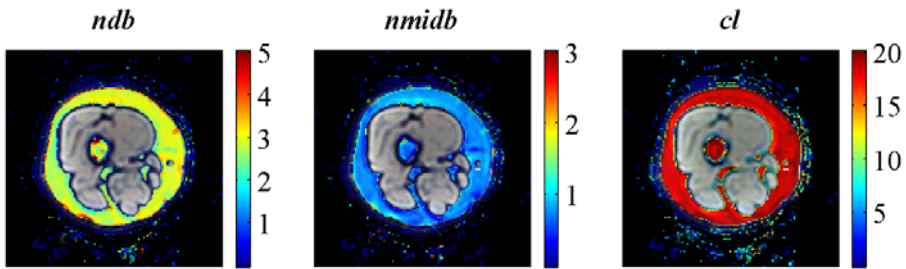

Figure 20. Example *ndb*, *nmidb*, and *cl* maps from the thigh of a healthy volunteer. The results in adipose tissue are overlaid on a raw data image. The average values of the estimated parameters in adipose tissue were: *ndb* = 2.83 ± 0.47, *nmidb* = 0.74 ± 0.17, and *cl* = 18.4 ± 1.4. (Paper IV)

7.4 Conclusions in summary

The potential and range of applications of MRI-based fat quantification techniques have been increased by the advances in this thesis. Specifically, the methods performance in low concentrations of fat has been evaluated, a novel method for quantification of the chemical composition of fat has been introduced, and a more efficient image acquisition strategy has been proven feasible for fat quantification. The conclusions in summary are:

1. Water/Fat Imaging makes the quantification of low fat concentrations (< 1 %) possible (**Paper I**). For fat quantification of low fat concentrations in

e.g. muscle tissue, the precision may be improved using a larger flip angle and a fat reference for quantification (**Paper II**).

2. The artifacts associated with a bipolar acquisition scheme are correctable using a built-in approach. Thus, the use of a bipolar acquisition scheme allows for more efficient image acquisition with high fat quantification accuracy and precision for most inter-echo shifts (**Paper III**).

3. Water/Fat Imaging and theoretical knowledge on the chemical structure of fat enables simultaneous image-based quantification of the fat content and the fatty acid composition (**Paper IV**). A long sampling time, careful consideration of the fat frequency model, modeling of individual fat and water T_2 values, and some T_1 weighting are recommended for accurate and noise efficient estimation of the fatty acid composition (**Paper V**).

Acknowledgements

Bakom varje rykande färsk avhandling står inte bara en darrande ny doktor (förhoppningsvis!) utan också ett stöttande team som hjälpt till med allt från vetenskap och datorer, till uppfostran och smutstvätt. Detta avsnitt är riktat till alla er!

Först av allt vill jag tacka min huvudhandledare: den oerhört tålmodige Sven. Stort tack för allt stöd och alla råd, din ofelbara tillgänglighet (även när du nog inte hade tid egentligen) och för att ingen fråga någonsin varit för liten eller för dum för att förtjäna din fulla uppmärksamhet. Jag har verkligen uppskattat att få jobba med dig de här åren!

Jag har också varit förunnad en hel massa biträdande handledare. Stort tack, Jonas, för råd och stöd, och för ditt sinne för den stora bilden. Tack, Håkan, för din entusiasm och för att din guidning i lymfödemvärlden. Tack, Peter, för hjälp och vägledning i anatomins och radiologins underbara värld. Tack, Sören, för det varma välkomnandet till avdelningen och för ditt inspirerande engagemang och aldrig sinande intresse. Tack också till nye professorn LEO för vägledning i allt från stort till smått.

När fysikern, mot sin vilja, famlar ut från sin kammare och möter verkligheten på kliniken har hjälpen från alla er på Röntgen varit fantastisk. Särskilt skulle jag vilja tacka Anetta för ordning och reda och alla ni vid kamerorna som gjort kliniska studier till ett rent nöje.

Ett stort tack riktas också till de andra svenska MR-fettforskarna: Thobias Romu, Olof Dahlqvist Leinhard, Joel Kullberg och Johan Berglund. Tack för att ni generöst delat med er av er kunskap!

Det har varit fantastiskt trevligt att arbeta på en avdelning med så många andra doktorander och kollegor inom olika områden; jag vill tacka er alla för trevligt sällskap och hjälp med allt möjligt. Särskilt vill jag tacka kontorskamraterna Marie, Calle, Elias och, även om det tyvärr blev kortvarigt, Marcus. Tack, Marie, för trevliga stunder av distraktion (ibland i form av ett par garnnystan) och för att du är en så fin vän som alltid ställer upp! Tack, Calle, för frysta kakor och massor av hjälp och diskussioner. Och, Elias, vi esteter måste ju hålla ihop. Tack för vänskapen!

Jag skulle även vilja tacka hela Lundagänget för alltid lika trevligt rese- och kurssällskap. Särskilt tack till Emelie för att du är en så god vän.

Tack också alla ni vänner utanför jobbet för att ni alltid åtminstone sett intresserade ut av hela den här magnetgrejen och för en hel massa glädje!

Jag vill tacka min familj för kärlek och omtanke; ni är så viktiga för mig! Tack min finaste mamma för allt du gör och för att du har ditt stora hjärta på vid gavel. Tack, Håkan, för din omtanke och för att du alltid ser min inre bohem. Tack, Cissi, för oändligt antal telefontimmar och för att du alltid säger exakt vad du tycker. Jag vill också skicka en tanke och en kram till min fina pappa och hans minne.

Slutligen vill jag tacka Erik: min kärlek, klippa och hem. Tack för allt du står ut med och för att du är just du och ingen annan.

References

Abate, N, Burns, D, Peshock, RM, Garg, A and Grundy, SM (1994). "Estimation of adipose tissue mass by magnetic resonance imaging: validation against dissection in human cadavers." *J Lipid Res* 35(8): 1490-1496.

Altman, DG and Bland, JM (1983). "Measurement in medicine: the analysis of method comparison studies." *The Statistician* 32: 307-317.

Artz, N, Hines, C, Brunner, S, Agni, R, Kuhn, JP, Roldan-Alzate, A, Chen, GH and Reeder, SB (2012). "Quantification of hepatic steatosis with dual-energy computed tomography: comparison with tissue reference standards and quantitative magnetic resonance imaging in the ob/ob mouse." *Invest Radiol* 47(10): 603-610.

Beasley, LE, Koster, A, Newman, AB, Javaid, MK, Ferrucci, L, Kritchevsky, SB, Kuller, LH, Pahor, M, Schaap, LA, Visser, M, Rubin, SM, Goodpaster, BH and Harris, TB (2009). "Inflammation and race and gender differences in computerized tomography-measured adipose depots." *Obesity (Silver Spring)* 17(5): 1062-1069.

Berglund, J, Ahlstrom, H and Kullberg, J (2012). "Model-based mapping of fat unsaturation and chain length by chemical shift imaging--phantom validation and in vivo feasibility." *Magn Reson Med* 68(6): 1815-1827.

Berglund, J, Johansson, L, Ahlstrom, H and Kullberg, J (2010). "Three-point Dixon method enables whole-body water and fat imaging of obese subjects." *Magn Reson Med* 63(6): 1659-1668.

Berglund, J and Kullberg, J (2012). "Three-dimensional water/fat separation and T2* estimation based on whole-image optimization--application in breathhold liver imaging at 1.5 T." *Magn Reson Med* 67(6): 1684-1693.

Bernard, CP, Liney, GP, Manton, DJ, Turnbull, LW and Langton, CM (2008). "Comparison of fat quantification methods: a phantom study at 3.0T." *J Magn Reson Imaging* 27(1): 192-197.

Bernstein, MA, King, KF and Zhou, XJ (2004). *Handbook of MRI Pulse Sequences*. San Diego, USA, Elsevier Academic Press.

Beynen, AC, Hermus, RJ and Hautvast, JG (1980). "A mathematical relationship between the fatty acid composition of the diet and that of the adipose tissue in man." *Am J Clin Nutr* 33(1): 81-85.

Blatter, DD, Morris, AH, Ailion, DC, Cutillo, AG and Case, TA (1985). "Asymmetric spin echo sequences. A simple new method for obtaining NMR 1H spectral images." *Invest Radiol* 20(8): 845-853.

Boesch, C, Slotboom, J, Hoppeler, H and Kreis, R (1997). "In vivo determination of intra-myocellular lipids in human muscle by means of localized 1H-MR-spectroscopy." *Magn Reson Med* 37(4): 484-493.

Boettcher, M, Machann, J, Stefan, N, Thamer, C, Haring, HU, Claussen, CD, Fritsche, A and Schick, F (2009). "Intermuscular adipose tissue (IMAT): association with other adipose tissue compartments and insulin sensitivity." *J Magn Reson Imaging* 29(6): 1340-1345.

Bohte, AE, van Werven, JR, Bipat, S and Stoker, J (2011). "The diagnostic accuracy of US, CT, MRI and 1H-MRS for the evaluation of hepatic steatosis compared with liver biopsy: a meta-analysis." *Eur Radiol* 21(1): 87-97.

Bottomley, PA (1987). "Spatial localization in NMR spectroscopy in vivo." *Ann N Y Acad Sci* 508: 333-348.

Brorson, H (2012). "From lymph to fat: liposuction as a treatment for complete reduction of lymphedema." *Int J Low Extrem Wounds* 11(1): 10-19.

Brorson, H, Ohlin, K, Olsson, G and Karlsson, MK (2009). "Breast cancer-related chronic arm lymphedema is associated with excess adipose and muscle tissue." *Lymphat Res Biol* 7(1): 3-10.

Brorson, H, Ohlin, K, Olsson, G and Nilsson, M (2006). "Adipose tissue dominates chronic arm lymphedema following breast cancer: an analysis using volume rendered CT images." *Lymphat Res Biol* 4(4): 199-210.

Brunt, EM, Janney, CG, Di Bisceglie, AM, Neuschwander-Tetri, BA and Bacon, BR (1999). "Nonalcoholic steatohepatitis: a proposal for grading and staging the histological lesions." *Am J Gastroenterol* 94(9): 2467-2474.

Buxton, RB, Wismer, GL, Brady, TJ and Rosen, BR (1986). "Quantitative proton chemical-shift imaging." *Magn Reson Med* 3(6): 881-900.

Bydder, M, Girard, O and Hamilton, G (2011). "Mapping the double bonds in triglycerides." *Magn Reson Imaging* 29(8): 1041-1046.

Bydder, M, Shiehmorteza, M, Yokoo, T, Sugay, S, Middleton, MS, Girard, O, Schroeder, ME, Wolfson, T, Gamst, A and Sirlin, C (2010). "Assessment of liver fat quantification in the presence of iron." *Magn Reson Imaging* 28(6): 767-776.

Bydder, M, Yokoo, T, Hamilton, G, Middleton, MS, Chavez, AD, Schwimmer, JB, Lavine, JE and Sirlin, CB (2008). "Relaxation effects in the quantification of fat using gradient echo imaging." *Magn Reson Imaging* 26(3): 347-359.

Capitan, V, Petit, JM, Aho, S, Lefevre, PH, Favelier, S, Loffroy, R, Hillon, P, Krause, D, Cercueil, JP and Guiu, B (2012). "Macroscopic heterogeneity of liver fat: an MR-based study in type-2 diabetic patients." *Eur Radiol* 22(10): 2161-2168.

Chebrolu, VV, Hines, CD, Yu, H, Pineda, AR, Shimakawa, A, McKenzie, CA, Samsonov, A, Brittain, JH and Reeder, SB (2010). "Independent estimation of T2* for water and fat for improved accuracy of fat quantification." *Magn Reson Med* 63(4): 849-857.

Clark, JM, Brancati, FL and Diehl, AM (2002). "Nonalcoholic fatty liver disease." *Gastroenterology* 122(6): 1649-1657.

Cui, Y, Yang, IY, Wade, T, Wiens, CN, Soliman, AS and McKenzie, CA (2012). "Absolute quantification of in vivo water and fat content" *20th Annual Meeting & Exhibition of the ISMRM*, Melbourne, Australia**:** 363.

Delmonico, MJ, Harris, TB, Visser, M, Park, SW, Conroy, MB, Velasquez-Mieyer, P, Boudreau, R, Manini, TM, Nevitt, M, Newman, AB and Goodpaster, BH (2009). "Longitudinal study of muscle strength, quality, and adipose tissue infiltration." *Am J Clin Nutr* 90(6): 1579-1585.

Dixon, WT (1984). "Simple proton spectroscopic imaging." *Radiology* 153(1): 189-194.

Doneva, M, Bornert, P, Eggers, H, Mertins, A, Pauly, J and Lustig, M (2010). "Compressed sensing for chemical shift-based water-fat separation." *Magn Reson Med* 64(6): 1749-1759.

Eggers, H, Brendel, B, Duijndam, A and Herigault, G (2011). "Dual-echo Dixon imaging with flexible choice of echo times." *Magn Reson Med* 65(1): 96-107.

Eggers, H, Koken, P and Börnert, P (2008). "Phase and Amplitude Correction in Bipolar Multi-Gradient-Echo Water-Fat Imaging" *16th Scientific Meeting and Exhibition of the ISMRM*, Toronto, USA**:** 1364.

Elliott, J, Pedler, A, Kenardy, J, Galloway, G, Jull, G and Sterling, M (2011). "The temporal development of fatty infiltrates in the neck muscles following whiplash injury: an association with pain and posttraumatic stress." *PLoS One* 6(6): e21194.

Frahm, J, Merboldt, KD and Hanicke, W (1987). "Localized Proton Spectroscopy Using Stimulated Echoes." *Journal of Magnetic Resonance* 72(3): 502-508.

Gallagher, D, Kuznia, P, Heshka, S, Albu, J, Heymsfield, SB, Goodpaster, B, Visser, M and Harris, TB (2005). "Adipose tissue in muscle: a novel depot similar in size to visceral adipose tissue." *Am J Clin Nutr* 81(4): 903-910.

Gerdle, B, Forsgren, MF, Bengtsson, A, Leinhard, OD, Soren, B, Karlsson, A, Brandejsky, V, Lund, E and Lundberg, P (2013). "Decreased muscle concentrations of ATP and PCR in the quadriceps muscle of fibromyalgia patients--a 31P-MRS study." *Eur J Pain* 17(8): 1205-1215.

Glover, GH (1991). "Multipoint Dixon technique for water and fat proton and susceptibility imaging." *J Magn Reson Imaging* 1(5): 521-530.

Gudbjartsson, H and Patz, S (1995). "The Rician distribution of noisy MRI data." *Magn Reson Med* 34(6): 910-914.

Guillén, MD and Ruiz, A (2003). "1H nuclear magnetic resonance as a fast tool for determining the composition of acyl chains in acylglycerol mixtures." *European Journal of Lipid Science and Technology* 105(9): 502-507.

Haase, A, Frahm, J, Hanicke, W and Matthaei, D (1985). "1H NMR chemical shift selective (CHESS) imaging." *Phys Med Biol* 30(4): 341-344.

Hamer, OW, Aguirre, DA, Casola, G, Lavine, JE, Woenckhaus, M and Sirlin, CB (2006). "Fatty liver: imaging patterns and pitfalls." *Radiographics* 26(6): 1637-1653.

Hamilton, G, Middleton, MS, Cunha, GM and Sirlin, CB (2013). "Effect of gadolinium-based contrast agent on the relaxation properties of water and fat in human liver as measured in

vivo by 1H MRS" *21st Annual Meeting and Exhibition of the ISMRM*, Salt Lake City, USA**:** 1516.

Hamilton, G, Smith, DL, Jr., Bydder, M, Nayak, KS and Hu, HH (2011). "MR properties of brown and white adipose tissues." *J Magn Reson Imaging* 34(2): 468-473.

Hamilton, G, Yokoo, T, Bydder, M, Cruite, I, Schroeder, ME, Sirlin, CB and Middleton, MS (2011). "In vivo characterization of the liver fat 1H MR spectrum." *NMR Biomed* 24(7): 784-790.

Hernando, D, Hines, CD, Yu, H and Reeder, SB (2012). "Addressing phase errors in fat-water imaging using a mixed magnitude/complex fitting method." *Magn Reson Med* 67(3): 638-644.

Hernando, D, Kellman, P, Haldar, JP and Liang, ZP (2010). "Robust water/fat separation in the presence of large field inhomogeneities using a graph cut algorithm." *Magn Reson Med* 63(1): 79-90.

Hernando, D, Liang, ZP and Kellman, P (2010). "Chemical shift-based water/fat separation: a comparison of signal models." *Magn Reson Med* 64(3): 811-822.

Hernando, D, Sharma, SD, Kramer, H and Reeder, SB (2013). "On the confounding effect of temperature on chemical shift-encoded fat quantification." *Magn Reson Med*.

Hines, CD, Agni, R, Roen, C, Rowland, I, Hernando, D, Bultman, E, Horng, D, Yu, H, Shimakawa, A, Brittain, JH and Reeder, SB (2012). "Validation of MRI biomarkers of hepatic steatosis in the presence of iron overload in the ob/ob mouse." *J Magn Reson Imaging* 35(4): 844-851.

Hines, CD, Frydrychowicz, A, Hamilton, G, Tudorascu, DL, Vigen, KK, Yu, H, McKenzie, CA, Sirlin, CB, Brittain, JH and Reeder, SB (2011). "T1 independent, T2* corrected chemical shift based fat-water separation with multi-peak fat spectral modeling is an accurate and precise measure of hepatic steatosis." *J Magn Reson Imaging* 33(4): 873-881.

Hines, CD, Yu, H, Shimakawa, A, McKenzie, CA, Brittain, JH and Reeder, SB (2009). "T1 independent, T2* corrected MRI with accurate spectral modeling for quantification of fat: validation in a fat-water-SPIO phantom." *J Magn Reson Imaging* 30(5): 1215-1222.

Hines, CD, Yu, H, Shimakawa, A, McKenzie, CA, Warner, TF, Brittain, JH and Reeder, SB (2010). "Quantification of hepatic steatosis with 3-T MR imaging: validation in ob/ob mice." *Radiology* 254(1): 119-128.

Hodson, L, Skeaff, CM and Fielding, BA (2008). "Fatty acid composition of adipose tissue and blood in humans and its use as a biomarker of dietary intake." *Prog Lipid Res* 47(5): 348-380.

Horng, DE, Hernando, D, Hines, CD and Reeder, SB (2013). "Comparison of R2* correction methods for accurate fat quantification in fatty liver." *J Magn Reson Imaging* 37(2): 414-422.

Hu, HH, Bornert, P, Hernando, D, Kellman, P, Ma, J, Reeder, S and Sirlin, C (2012). "ISMRM workshop on fat-water separation: insights, applications and progress in MRI." *Magn Reson Med* 68(2): 378-388.

Hu, HH, Kim, HW, Nayak, KS and Goran, MI (2010). "Comparison of fat-water MRI and single-voxel MRS in the assessment of hepatic and pancreatic fat fractions in humans." *Obesity (Silver Spring)* 18(4): 841-847.

Hu, HH, Li, Y, Nagy, TR, Goran, MI and Nayak, KS (2011). "Quantification of absolute fat mass by magnetic resonance imaging: a validation study against chemical analysis." *Int J Body Compos Res* 9(3): 111-122.

Hu, HH and Nayak, KS (2008). "Quantification of absolute fat mass using an adipose tissue reference signal model." *J Magn Reson Imaging* 28(6): 1483-1491.

Hu, HH and Nayak, KS (2010). "Change in the proton T1 of fat and water in mixture." *Magn Reson Med* 63(2): 494-501.

Hwang, JH, Pan, JW, Heydari, S, Hetherington, HP and Stein, DT (2001). "Regional differences in intramyocellular lipids in humans observed by in vivo 1H-MR spectroscopic imaging." *J Appl Physiol (1985)* 90(4): 1267-1274.

ICRP (2002). "Basic anatomical and physiological data for use in radiological protection: reference values. A report of age- and gender-related differences in the anatomical and physiological characteristics of reference individuals. ICRP Publication 89." *Ann ICRP* 32(3-4): 5-265.

Iggman, D, Arnlov, J, Vessby, B, Cederholm, T, Sjogren, P and Riserus, U (2010). "Adipose tissue fatty acids and insulin sensitivity in elderly men." *Diabetologia* 53(5): 850-857.

Kang, BK, Yu, ES, Lee, SS, Lee, Y, Kim, N, Sirlin, CB, Cho, EY, Yeom, SK, Byun, JH, Park, SH and Lee, MG (2012). "Hepatic fat quantification: a prospective comparison of magnetic resonance spectroscopy and analysis methods for chemical-shift gradient echo magnetic resonance imaging with histologic assessment as the reference standard." *Invest Radiol* 47(6): 368-375.

Kang, GH, Cruite, I, Shiehmorteza, M, Wolfson, T, Gamst, AC, Hamilton, G, Bydder, M, Middleton, MS and Sirlin, CB (2011). "Reproducibility of MRI-determined proton density fat fraction across two different MR scanner platforms." *J Magn Reson Imaging* 34(4): 928-934.

Karampinos, DC, Baum, T, Nardo, L, Alizai, H, Yu, H, Carballido-Gamio, J, Yap, SP, Shimakawa, A, Link, TM and Majumdar, S (2012). "Characterization of the regional distribution of skeletal muscle adipose tissue in type 2 diabetes using chemical shift-based water/fat separation." *J Magn Reson Imaging* 35(4): 899-907.

Karampinos, DC, Yu, H, Shimakawa, A, Link, TM and Majumdar, S (2011). "T1-corrected fat quantification using chemical shift-based water/fat separation: application to skeletal muscle." *Magn Reson Med* 66(5): 1312-1326.

Karampinos, DC, Yu, H, Shimakawa, A, Link, TM and Majumdar, S (2012). "Chemical shift-based water/fat separation in the presence of susceptibility-induced fat resonance shift." *Magn Reson Med* 68(5): 1495-1505.

Kellman, P, Hernando, D and Arai, AE (2010). "Myocardial Fat Imaging." *Curr Cardiovasc Imaging Rep* 3(2): 83-91.

Kleiner, DE, Brunt, EM, Van Natta, M, Behling, C, Contos, MJ, Cummings, OW, Ferrell, LD, Liu, YC, Torbenson, MS, Unalp-Arida, A, Yeh, M, McCullough, AJ and Sanyal, AJ (2005). "Design and validation of a histological scoring system for nonalcoholic fatty liver disease." *Hepatology* 41(6): 1313-1321.

Knight, WD (1949). "Nuclear magnetic resonance shift in metals." *Physical Review* 76(8): 1259-1260.

Krssak, M, Mlynarik, V, Meyerspeer, M, Moser, E and Roden, M (2004). "1H NMR relaxation times of skeletal muscle metabolites at 3 T." *MAGMA* 16(4): 155-159.

Kuroda, K, Oshio, K, Chung, AH, Hynynen, K and Jolesz, FA (1997). "Temperature mapping using the water proton chemical shift: a chemical shift selective phase mapping method." *Magn Reson Med* 38(5): 845-851.

Leander, P, Sjoberg, S and Hoglund, P (2000). "CT and MR imaging of the liver. Clinical importance of nutritional status." *Acta Radiol* 41(2): 151-155.

Lee, Y, Jee, HJ, Noh, H, Kang, GH, Park, J, Cho, J, Cho, JH, Ahn, S, Lee, C, Kim, OH, Oh, BC and Kim, H (2012). "In vivo 1H-MRS hepatic lipid profiling in nonalcoholic fatty liver disease: An animal study at 9.4 T." *Magn Reson Med* 70(3): 620-629.

Leinhard, OD, Johansson, A, Rydell, J, Smedby, O, Nystrom, F, Lundberg, P and Borga, M (2008). "Quantitative abdominal fat estimation using MRI." *19th International Conference on Pattern Recognition, Vols 1-6*: 2137-2140.

Leupold, J, Wieben, O, Mansson, S, Speck, O, Scheffler, K, Petersson, JS and Hennig, J (2006). "Fast chemical shift mapping with multiecho balanced SSFP." *MAGMA* 19(5): 267-273.

Li, Z, Gmitro, AF, Bilgin, A and Altbach, MI (2007). "Fast decomposition of water and lipid using a GRASE technique with the IDEAL algorithm." *Magn Reson Med* 57(6): 1047-1057.

Liu, CY, McKenzie, CA, Yu, H, Brittain, JH and Reeder, SB (2007). "Fat quantification with IDEAL gradient echo imaging: correction of bias from T1 and noise." *Magn Reson Med* 58(2): 354-364.

Liu, CY, Redheuil, A, Ouwerkerk, R, Lima, JA and Bluemke, DA (2010). "Myocardial fat quantification in humans: Evaluation by two-point water-fat imaging and localized proton spectroscopy." *Magn Reson Med* 63(4): 892-901.

Lodes, CC, Felmlee, JP, Ehman, RL, Sehgal, CM, Greenleaf, JF, Glover, GH and Gray, JE (1989). "Proton MR chemical shift imaging using double and triple phase contrast acquisition methods." *J Comput Assist Tomogr* 13(5): 855-861.

Longo, R, Pollesello, P, Ricci, C, Masutti, F, Kvam, BJ, Bercich, L, Croce, LS, Grigolato, P, Paoletti, S, de Bernard, B and et al. (1995). "Proton MR spectroscopy in quantitative in vivo determination of fat content in human liver steatosis." *J Magn Reson Imaging* 5(3): 281-285.

Lu, W, Yu, H, Shimakawa, A, Alley, M, Reeder, SB and Hargreaves, BA (2008). "Water-fat separation with bipolar multiecho sequences." *Magn Reson Med* 60(1): 198-209.

Lundbom, J, Hakkarainen, A, Lundbom, N and Taskinen, MR (2013). "Deep subcutaneous adipose tissue is more saturated than superficial subcutaneous adipose tissue." *Int J Obes (Lond)* 37(4): 620-622.

Lundbom, J, Hakkarainen, A, Soderlund, S, Westerbacka, J, Lundbom, N and Taskinen, MR (2011). "Long-TE 1H MRS suggests that liver fat is more saturated than subcutaneous and visceral fat." *NMR Biomed* 24(3): 238-245.

Ma, J (2004). "Breath-hold water and fat imaging using a dual-echo two-point Dixon technique with an efficient and robust phase-correction algorithm." *Magn Reson Med* 52(2): 415-419.

Machann, J, Thamer, C, Schnoedt, B, Haap, M, Haring, HU, Claussen, CD, Stumvoll, M, Fritsche, A and Schick, F (2005). "Standardized assessment of whole body adipose tissue topography by MRI." *J Magn Reson Imaging* 21(4): 455-462.

Madden, MC, Van Winkle, WB, Kirk, K, Pike, MM, Pohost, GM and Wolkowicz, PE (1993). "1H-NMR spectroscopy can accurately quantitate the lipolysis and oxidation of cardiac triacylglycerols." *Biochim Biophys Acta* 1169(2): 176-182.

Malcom, GT, Bhattacharyya, AK, Velez-Duran, M, Guzman, MA, Oalmann, MC and Strong, JP (1989). "Fatty acid composition of adipose tissue in humans: differences between subcutaneous sites." *Am J Clin Nutr* 50(2): 288-291.

Mattsson, S and Thomas, BJ (2006). "Development of methods for body composition studies." *Phys Med Biol* 51(13): R203-228.

Maudsley, A, Hilal, S, Perman, W and Simon, H (1983). "Spatially resolved high resolution spectroscopy by "four-dimensional" NMR." *Journal of Magnetic Resonance (1969)* 51(1): 147-152.

McGavock, JM, Lingvay, I, Zib, I, Tillery, T, Salas, N, Unger, R, Levine, BD, Raskin, P, Victor, RG and Szczepaniak, LS (2007). "Cardiac steatosis in diabetes mellitus: a 1H-magnetic resonance spectroscopy study." *Circulation* 116(10): 1170-1175.

Meisamy, S, Hines, CD, Hamilton, G, Sirlin, CB, McKenzie, CA, Yu, H, Brittain, JH and Reeder, SB (2011). "Quantification of hepatic steatosis with T1-independent, T2-corrected MR imaging with spectral modeling of fat: blinded comparison with MR spectroscopy." *Radiology* 258(3): 767-775.

Meyer, CH, Pauly, JM, Macovski, A and Nishimura, DG (1990). "Simultaneous spatial and spectral selective excitation." *Magn Reson Med* 15(2): 287-304.

Perez Perez, A, Ybarra Munoz, J, Blay Cortes, V and de Pablos Velasco, P (2007). "Obesity and cardiovascular disease." *Public Health Nutr* 10(10A): 1156-1163.

Pineda, AR, Reeder, SB, Wen, Z and Pelc, NJ (2005). "Cramer-Rao bounds for three-point decomposition of water and fat." *Magn Reson Med* 54(3): 625-635.

Pond, CM (2005). "Adipose tissue and the immune system." *Prostaglandins Leukot Essent Fatty Acids* 73(1): 17-30.

Rasouli, N, Molavi, B, Elbein, SC and Kern, PA (2007). "Ectopic fat accumulation and metabolic syndrome." *Diabetes Obes Metab* 9(1): 1-10.

Ratziu, V, Charlotte, F, Heurtier, A, Gombert, S, Giral, P, Bruckert, E, Grimaldi, A, Capron, F, Poynard, T and Group, LS (2005). "Sampling variability of liver biopsy in nonalcoholic fatty liver disease." *Gastroenterology* 128(7): 1898-1906.

Reeder, SB, Bice, EK, Yu, H, Hernando, D and Pineda, AR (2012). "On the performance of T2* correction methods for quantification of hepatic fat content." *Magn Reson Med* 67(2): 389-404.

Reeder, SB, Cruite, I, Hamilton, G and Sirlin, CB (2011). "Quantitative assessment of liver fat with magnetic resonance imaging and spectroscopy." *J Magn Reson Imaging* 34(4): 729-749.

Reeder, SB, McKenzie, CA, Pineda, AR, Yu, H, Shimakawa, A, Brau, AC, Hargreaves, BA, Gold, GE and Brittain, JH (2007). "Water-fat separation with IDEAL gradient-echo imaging." *J Magn Reson Imaging* 25(3): 644-652.

Reeder, SB, Robson, PM, Yu, H, Shimakawa, A, Hines, CD, McKenzie, CA and Brittain, JH (2009). "Quantification of hepatic steatosis with MRI: the effects of accurate fat spectral modeling." *J Magn Reson Imaging* 29(6): 1332-1339.

Reeder, SB, Wen, Z, Yu, H, Pineda, AR, Gold, GE, Markl, M and Pelc, NJ (2004). "Multicoil Dixon chemical species separation with an iterative least-squares estimation method." *Magn Reson Med* 51(1): 35-45.

Rockson, SG (2013). "The lymphatics and the inflammatory response: lessons learned from human lymphedema." *Lymphat Res Biol* 11(3): 117-120.

Roldan-Valadez, E, Favila, R, Martinez-Lopez, M, Uribe, M, Rios, C and Mendez-Sanchez, N (2010). "In vivo 3T spectroscopic quantification of liver fat content in nonalcoholic fatty liver disease: Correlation with biochemical method and morphometry." *J Hepatol* 53(4): 732-737.

Romu, T, Borga, M and Leinhard, OD (2011). "Mana - Multi scale adaptive normalized averaging." *2011 8th IEEE International Symposium on Biomedical Imaging: From Nano to Macro*: 361-364.

Scharf, LL and McWhorter, LT (1993). "Geometry of the Cramer-Rao bound." *Signal Processing* 31(3): 301-311.

Schick, F, Machann, J, Brechtel, K, Strempfer, A, Klumpp, B, Stein, DT and Jacob, S (2002). "MRI of muscular fat." *Magn Reson Med* 47(4): 720-727.

Schrauwen-Hinderling, VB, Hesselink, MK, Schrauwen, P and Kooi, ME (2006). "Intramyocellular lipid content in human skeletal muscle." *Obesity (Silver Spring)* 14(3): 357-367.

Schwenzer, NF, Springer, F, Schraml, C, Stefan, N, Machann, J and Schick, F (2009). "Non-invasive assessment and quantification of liver steatosis by ultrasound, computed tomography and magnetic resonance." *J Hepatol* 51(3): 433-445.

Sepponen, RE, Sipponen, JT and Tanttu, JI (1984). "A method for chemical shift imaging: demonstration of bone marrow involvement with proton chemical shift imaging." *J Comput Assist Tomogr* 8(4): 585-587.

Shen, W, Wang, Z, Punyanita, M, Lei, J, Sinav, A, Kral, JG, Imielinska, C, Ross, R and Heymsfield, SB (2003). "Adipose tissue quantification by imaging methods: a proposed classification." *Obes Res* 11(1): 5-16.

Snel, M, Jonker, JT, Schoones, J, Lamb, H, de Roos, A, Pijl, H, Smit, JW, Meinders, AE and Jazet, IM (2012). "Ectopic fat and insulin resistance: pathophysiology and effect of diet and lifestyle interventions." *Int J Endocrinol* 2012: 983814.

Stark, DD and Bradley, WG (1992). *Magnetic resonance imaging*. St. Louis, Mosby-Year Book.

Staten, MA, Totty, WG and Kohrt, WM (1989). "Measurement of fat distribution by magnetic resonance imaging." *Invest Radiol* 24(5): 345-349.

Strauss, S, Gavish, E, Gottlieb, P and Katsnelson, L (2007). "Interobserver and intraobserver variability in the sonographic assessment of fatty liver." *AJR Am J Roentgenol* 189(6): W320-323.

Szczepaniak, LS, Babcock, EE, Schick, F, Dobbins, RL, Garg, A, Burns, DK, McGarry, JD and Stein, DT (1999). "Measurement of intracellular triglyceride stores by H spectroscopy: validation in vivo." *Am J Physiol* 276(5 Pt 1): E977-989.

Szczepaniak, LS, Dobbins, RL, Stein, DT and McGarry, JD (2002). "Bulk magnetic susceptibility effects on the assessment of intra- and extramyocellular lipids in vivo." *Magn Reson Med* 47(3): 607-610.

Szczepaniak, LS, Nurenberg, P, Leonard, D, Browning, JD, Reingold, JS, Grundy, S, Hobbs, HH and Dobbins, RL (2005). "Magnetic resonance spectroscopy to measure hepatic triglyceride content: prevalence of hepatic steatosis in the general population." *Am J Physiol Endocrinol Metab* 288(2): E462-468.

van Werven, JR, Marsman, HA, Nederveen, AJ, Smits, NJ, ten Kate, FJ, van Gulik, TM and Stoker, J (2010). "Assessment of hepatic steatosis in patients undergoing liver resection: comparison of US, CT, T1-weighted dual-echo MR imaging, and point-resolved 1H MR spectroscopy." *Radiology* 256(1): 159-168.

van Werven, JR, Marsman, HA, Nederveen, AJ, ten Kate, FJ, van Gulik, TM and Stoker, J (2012). "Hepatic lipid composition analysis using 3.0-T MR spectroscopy in a steatotic rat model." *Magn Reson Imaging* 30(1): 112-121.

Wiens, CN, Addeman, BT, Kisch, SJ, Hines, CD, Yu, H, Brittain, JH, Reeder, SB and McKenzie, CA (2009). "Quantification of Noise Efficiency with T1 corrected IDEAL Spoiled Gradient Echo Imaging" *17th Annual Meeting & Exhibition of the ISMRM*, Honolulu, USA**:** 363.

World Health Organization. (2013). "Obesity and Overweight Fact Sheet No 311."

Vuppalanchi, R, Cummings, OW, Saxena, R, Ulbright, TM, Martis, N, Jones, DR, Bansal, N and Chalasani, N (2007). "Relationship among histologic, radiologic, and biochemical assessments of hepatic steatosis: a study of human liver samples." *J Clin Gastroenterol* 41(2): 206-210.

Xiang, QS and An, L (1997). "Water-fat imaging with direct phase encoding." *J Magn Reson Imaging* 7(6): 1002-1015.

Yang, IY, Cui, Y, Wiens, CN, Wade, TP, Friesen-Waldner, LJ and McKenzie, CA (2013). "Fat fraction bias correction using T1 estimates and flip angle mapping." *J Magn Reson Imaging*.

Yang, K (2008). *Adipose tissue protocols*. Totowa, N.J., Humana.

Yu, H, McKenzie, CA, Shimakawa, A, Vu, AT, Brau, AC, Beatty, PJ, Pineda, AR, Brittain, JH and Reeder, SB (2007). "Multiecho reconstruction for simultaneous water-fat decomposition and T2* estimation." *J Magn Reson Imaging* 26(4): 1153-1161.

Yu, H, Reeder, SB, Shimakawa, A, Brittain, JH and Pelc, NJ (2005). "Field map estimation with a region growing scheme for iterative 3-point water-fat decomposition." *Magn Reson Med* 54(4): 1032-1039.

Yu, H, Shimakawa, A, Hines, CD, McKenzie, CA, Hamilton, G, Sirlin, CB, Brittain, JH and Reeder, SB (2011). "Combination of complex-based and magnitude-based multiecho water-fat separation for accurate quantification of fat-fraction." *Magn Reson Med* 66(1): 199-206.

Yu, H, Shimakawa, A, McKenzie, CA, Brodsky, E, Brittain, JH and Reeder, SB (2008). "Multiecho water-fat separation and simultaneous R2* estimation with multifrequency fat spectrum modeling." *Magn Reson Med* 60(5): 1122-1134.

Yu, H, Shimakawa, A, McKenzie, CA, Lu, W, Reeder, SB, Hinks, RS and Brittain, JH (2010). "Phase and amplitude correction for multi-echo water-fat separation with bipolar acquisitions." *J Magn Reson Imaging* 31(5): 1264-1271.

Yu, H, Shimakawa, A, McKenzie, CA, Vu, AT, Brau, AC, Beatty, PJ, Reeder, SB and Brittain, JH (2007). *A Multi-echo Acquisition Method with Reduced Echo Spacing for Robust IDEAL Water-Fat Decomposition at 3T*. Joint Annual Meeting ISMRM-ESMRMB, Berlin, Germany.

Zoico, E, Rossi, A, Di Francesco, V, Sepe, A, Olioso, D, Pizzini, F, Fantin, F, Bosello, O, Cominacini, L, Harris, TB and Zamboni, M (2010). "Adipose tissue infiltration in skeletal muscle of healthy elderly men: relationships with body composition, insulin resistance, and inflammation at the systemic and tissue level." *J Gerontol A Biol Sci Med Sci* 65(3): 295-299.